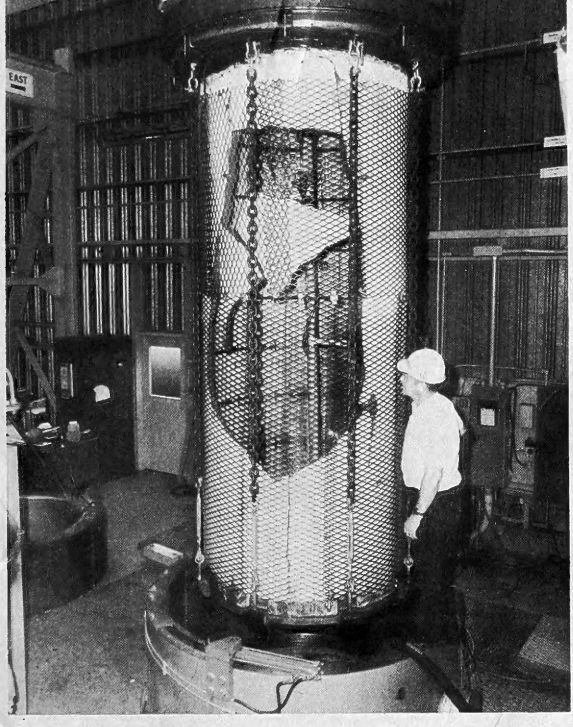

R874

TECHNICAL REPORT
CIVIL ENGINEERING LABORATORY

Naval Construction Battalion Center, Port Hueneme, California 93043

DESIGN FOR IMPLOSION OF CONCRETE CYLINDER STRUCTURES UNDER HYDROSTATIC LOADING

By

Harvey H. Haynes

August 1979

ed by

FACILITIES ENGINEERING COMMAND

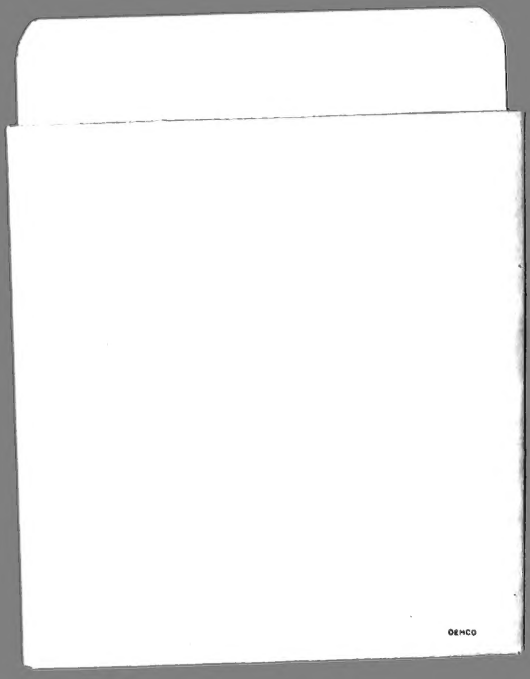

Unclassified

SECURITY CLASSIFICATION OF THIS PAGE *(When Data Entered)*

REPORT DOCUMENTATION PAGE		READ INSTRUCTIONS BEFORE COMPLETING FORM
1. REPORT NUMBER TR-874	2. GOVT ACCESSION NO. DN044053	3. RECIPIENT'S CATALOG NUMBER
4. TITLE *(and Subtitle)* DESIGN FOR IMPLOSION OF CONCRETE CYLINDER STRUCTURES UNDER HYDROSTATIC LOADING		5. TYPE OF REPORT & PERIOD COVERED Not final; Jul 78 - Mar 79 6. PERFORMING ORG. REPORT NUMBER
7. AUTHOR(s) Harvey H. Haynes		8. CONTRACT OR GRANT NUMBER(s)
9. PERFORMING ORGANIZATION NAME AND ADDRESS CIVIL ENGINEERING LABORATORY Naval Construction Battalion Center Port Hueneme, California 93043		10. PROGRAM ELEMENT, PROJECT, TASK AREA & WORK UNIT NUMBERS 3.1610-1
11. CONTROLLING OFFICE NAME AND ADDRESS Naval Facilities Engineering Command Alexandria, Virginia 22332		12. REPORT DATE August 1979 13. NUMBER OF PAGES 85
14. MONITORING AGENCY NAME & ADDRESS*(if different from Controlling Office)*		15. SECURITY CLASS. *(of this report)* Unclassified 15a. DECLASSIFICATION/DOWNGRADING SCHEDULE

16. DISTRIBUTION STATEMENT *(of this Report)*

Approved for public release; distribution unlimited.

17. DISTRIBUTION STATEMENT *(of the abstract entered in Block 20, if different from Report)*

18. SUPPLEMENTARY NOTES

19. KEY WORDS *(Continue on reverse side if necessary and identify by block number)*

Concrete structures, pressure-resistant structures, concrete cylinders, implosion, submerged concrete structures, undersea structures, unreinforced concrete, hydrostatic loading, design guidelines, buckling.

20. ABSTRACT *(Continue on reverse side if necessary and identify by block number)*

This report presents updated design guides for both thick- and thin-walled concrete cylinder structures under hydrostatic loading. The design approach for thick-walled cylinders has been changed from that described in previous work to a semi-empirical basis; improvements in implosion strength on the order of 10% are found. A test on a thick-walled 10-ft-diam (3.05-m) structure loaded to failure in the ocean is reported. A major change in the guides is

continued

DD FORM 1 JAN 73 1473 EDITION OF 1 NOV 65 IS OBSOLETE

Unclassified

SECURITY CLASSIFICATION OF THIS PAGE *(When Data Entered)*

20. Continued

for thin-walled cylinders, where new data on 15 relatively large-scale specimens are reported. Design guides for thin-walled cylinders show an increase in implosion strength ranging from 0% to 35%, depending on the structures' t/D_o and L/D_o ratios, from that reported previously.

Library Card

Civil Engineering Laboratory
DESIGN FOR IMPLOSION OF CONCRETE CYLINDER STRUCTURES UNDER HYDROSTATIC LOADING,
by Harvey H. Haynes
TR-874 85 pp illus Aug 1979 Unclassified

1. Concrete cylinders 2. Hydrostatic loadings I. 3.1610-1

This report presents updated design guides for both thick- and thin-walled concrete cylinder structures under hydrostatic loading. The design approach for thick-walled cylinders has been changed from that described in previous work to a semi-empirical basis; improvements in implosion strength on the order of 10% are found. A test on a thick-walled 10-ft-diam (3.05-m) structure loaded to failure in the ocean is reported. A major change in the guides is for thin-walled cylinders, where new data on 15 relatively large-scale specimens are reported. Design guides for thin-walled cylinders show an increase in implosion strength ranging from 0% to 35%, depending on the structures' t/D_o and L/D_o ratios, from that reported previously.

CONTENTS

INTRODUCTION

Background

In the mid-1960's ocean engineering attracted considerable interest in research and development on providing man with the technology to work in the deep ocean. Research on undersea concrete structures was initiated at this time, and exploratory test results showed much promise (Ref 1) for concrete structures at depths to 3,000 feet (1,000 meters). The economic payoff of the research was that massive undersea concrete structures would cost about one-tenth that of metallic structures.

For the first several years, research was directed solely to concrete spheres, but tests on cylinders started about 1970. The early cylinder models had an outside diameter of 16 inches (406 mm). Parameters such as cylinder length, wall thickness, end closure conditions, and concrete compressive strength (Ref 2 to 4) were investigated and studied.

The North Sea oil boom occurred in the early 1970's, and the first offshore concrete platform, called Ekofisk, was built. With the successful installation of Ekofisk in a water depth of 270 feet (90 meters), industry ordered additional concrete structures for oil drilling and production. A dynamic development period ensued during which it became apparent that knowledge on the behavior of pressure-resistant concrete structures was substantially lacking.

In an attempt to make existing data known, Civil Engineering Laboratory (CEL) test results were distributed widely (Ref 5 to 8). However, the early work on cylinder structures was quite tentative because of limited data on thin-walled cylinders.

A major oil company proposed a test program on large-scale, thin-walled concrete models. This proposal eventually led to a joint industry-Navy test program carried out at CEL.

During this period another important test was conducted at CEL on a large thick-walled concrete cylinder structure. The structure, called SEACON I, was part of an integrated seafloor engineering experiment to demonstrate capability in constructing operational facilities in the ocean (Ref 9). The structure was built in 1972, placed in the ocean at 600 feet (180 meters) for 10 months, and then retrieved. After being on "display" for several years, it was tested to failure in the ocean in 1976 to determine its implosion strength.

Objective

This report presents updated design guides for implosion of concrete cylinders. The guides are based on the test results from the thick-walled, SEACON I, cylinder test (Appendix A) and from the thin-walled cylinder tests (Appendix B). The approach to design is similar to that already presented in Reference 8. However, the new data are superior to that presented previously, especially for the thin-walled models. The updated guides for thin-walled cylinders allow such structures to operate at considerably deeper depths than indicated in the past guides.

Description of Tests

Thick-Walled Structures. The SEACON I structure was a reinforced concrete cylindrical hull having hemispherical end closures. The overall structure length was 20 feet (6.1 meters); outside diameter, 10.1 feet (3.08 meters); and wall thickness, 9.5 inches (241 mm). Steel reinforcement of 0.7% by area was used in both the hoop and axial directions. At the time of the implosion test the concrete compressive strength was 10,470 psi.

During the long-term loading test of the structure at 600 feet, results were obtained on the structure's response from initial loading and creep. Although the data are interesting, the pressure load was relatively low, only 14% of its ultimate strength. Of more significance was the implosion test where the structure was lowered into the ocean until failure. Complications occurred during this test which precluded obtaining structural response data, but the implosion pressure was successfully obtained. This test with its results is presented in Appendix A.

Thin-Walled Structures. The thin-walled cylinder test program encompassed 15 unreinforced concrete specimens, whose dimensions were: 134 inches (3.4 meters) length, 54 inches (1372 mm) OD, and 1.31, 1.97, or 3.39 inches (33, 50, or 86 mm, respectively) wall thickness. Two different boundary conditions were modeled, a free and a simple support, in order that cylinders of two effective lengths could be studied. The concrete compressive strength ranged between a nominal 7,000 to 8,000 psi (48 to 55 MPa).

Structural deformations were monitored by recording radial displacements around the circumference of the cylinder. Accurate initial and deflected cross-sectional shapes were obtained which showed the progressive development of out-of-roundness.

An analytical study using actual material properties and geometric conditions was conducted. A finite-element analysis with an advanced constitutive material model was used.

This test program on thin-walled cylinders is presented in Appendix B.

DESIGN FOR IMPLOSION

Thick-Walled Cylinders

The design approach for unreinforced, thick-walled cylinders is based on an average stress distribution across the wall of the cylinder

at implosion. Near implosion, the inelastic behavior of concrete along with plasticity and creep impart a stress distribution across the wall that is more closely modeled by a uniform stress distribution than by an elastic (Lamé) stress distribution. A uniform stress at implosion is expressed by

$$\sigma_{im} = P_{im} \frac{R_o}{t} \tag{1}$$

where σ_{im} = wall stress at implosion
p_{im} = implosion pressure
R_o = outside radius
t = average wall thickness

The wall stress at implosion, σ_{im}, can be expressed as the ultimate compressive strength of concrete multiplied by a strength factor.

$$\sigma_{im} = k_c f'_c \tag{2}$$

where k_c = strength factor for cylinder structures under hydrostatic loading
f'_c = uniaxial compressive strength of concrete

The term k_c was determined empirically. Figure 1 shows k_c as a function of length-to-outside-diameter ratio, L/D_o, for cylinders of various wall-thickness-to-outside-diameter ratios, t/D_o.

For cylinders under hydrostatic loading, the wall is stressed biaxially in compression on the inside surface and triaxially in compression at all other locations. The two major stresses are in the hoop and axial direction where the hoop stress is about twice the magnitude of the axial stress. The third, and smallest, component of stress acts radially. If the concrete is considered biaxially loaded, then the hoop-to-axial stress ratio of 2 is known to increase the compressive strength

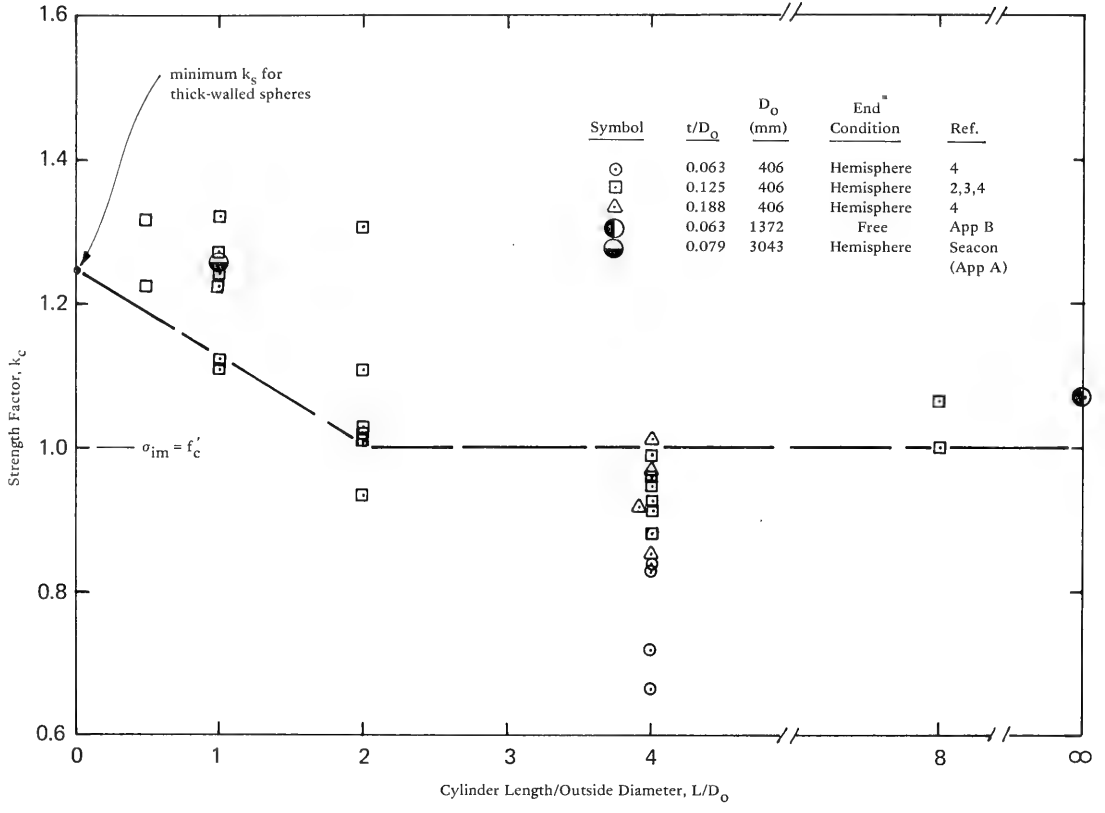

Figure 1. Relationship between k_c and L/D_o for thick-walled cylinders.

of concrete by a factor of about 1.25 f'_c (Ref 10). Therefore, k_c values for the cylinder test specimen of this program should show a value on the order of 1.25. As a minimum, k_c should be 1.0.

Figure 1 shows that short cylinders, those of $L/D_o \leq 1$, had a k_c around 1.25. However, longer cylinders showed a k_c on the order of 1.0. The decrease in k_c was probably due to specimen imperfection. The short specimens were also imperfect, but end-closure effects restrained the cylinder wall. At L/D_o of 2.0 the end-closure effects were diminished.

An average k_c value of 0.89 was observed at $L/D_o = 4$. It was speculated that some unknown fabrication or testing problem existed for the cylinders of this length in comparison to the other specimens.*

For design purposes, a $k_c = 1.0$ was selected for cylinders of $L/D_o \geq 2$. The reader is reminded that this k_c includes the effect of out-of-roundness and experimental error. The reduction in k_c from 1.25 to 1.0, a 20% change, is difficult to assign solely to out-of-roundness effect because thick-walled structures are usually insensitive to small geometric out-of-roundness. Hence, $k_c = 1.0$ should be a conservative strength factor for design purposes.

*Much attention was given to why k_c should be as low as 0.89. If out-of-roundness was the sole cause, then the specimens showed a decrease in strength of 29% due to out-of-roundness, which was too large an effect for thick-walled cylinders. There appeared to be no reason based on engineering mechanics to cause cylinders with L/D_o of 4 to fail at lower pressures than those at, say, L/D_o of 8. It is believed that some problem related to specimen fabrication or test was responsible for the low strengths. The author personally participated in the fabrication and testing of some of the specimens under consideration. He discussed this topic with others involved in the test program, and no procedure was singled out as suspicious. One procedure that was distinctly different for specimens of L/D_o of 4 and 8 from that of the shorter specimens related to the interior mold. The interior mold was made in segments having a length of $L/D_o = 2$. Cylinders longer than L/D_o of 2 used multiple segments. During mold removal operations it was quite difficult to disassemble the multiple segments to extract the interior mold. If harm was done to the specimens during this operation, it was not recognized at the time.

Although the cylinders were fabricated in rigid steel molds (Ref 2), the mold segments sprang slightly after the first disassembly. After References 2 and 4 were already published, a short cylinder section was mounted in a lathe to determine out-of-roundness more accurately than had been done previously. The inside and outside radius and the wall thickness varied by ±1/32 inch (1.6 mm). The out-of-roundness parameters are summarized in Table 1.

Substituting Equation 2 into Equation 1 and using $R_o = D_o/2$ gives the expression to predict implosion pressure for thick-walled cylinders:

$$P_{im} = 2\, k_c\, f'_c\, (t/D_o) \qquad (3)$$

where $k_c = 1.25 - 0.12(L/D_o)$ for $L/D_o < 2$

$k_c = 1.0$ for $L/D_o \geq 2$

Equation 3 is shown in Figure 2, which can be used as a design chart.

A more general design chart approach is shown in Figure 3. The chart is entered with a cylinder L/D_o and t/D_o to obtain the P_{im}/f'_c ratio. The implosion pressure can then be calculated by assuming a concrete compressive strength, f'_c.

The effect of different types of end-closures on the implosion strength was judged to be small (Ref 3) so this parameter was not included in the design equation.

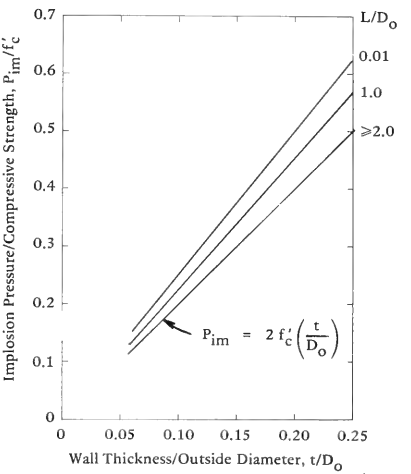

Figure 2. Relationship of Equation 3 for thick-walled cylinders.

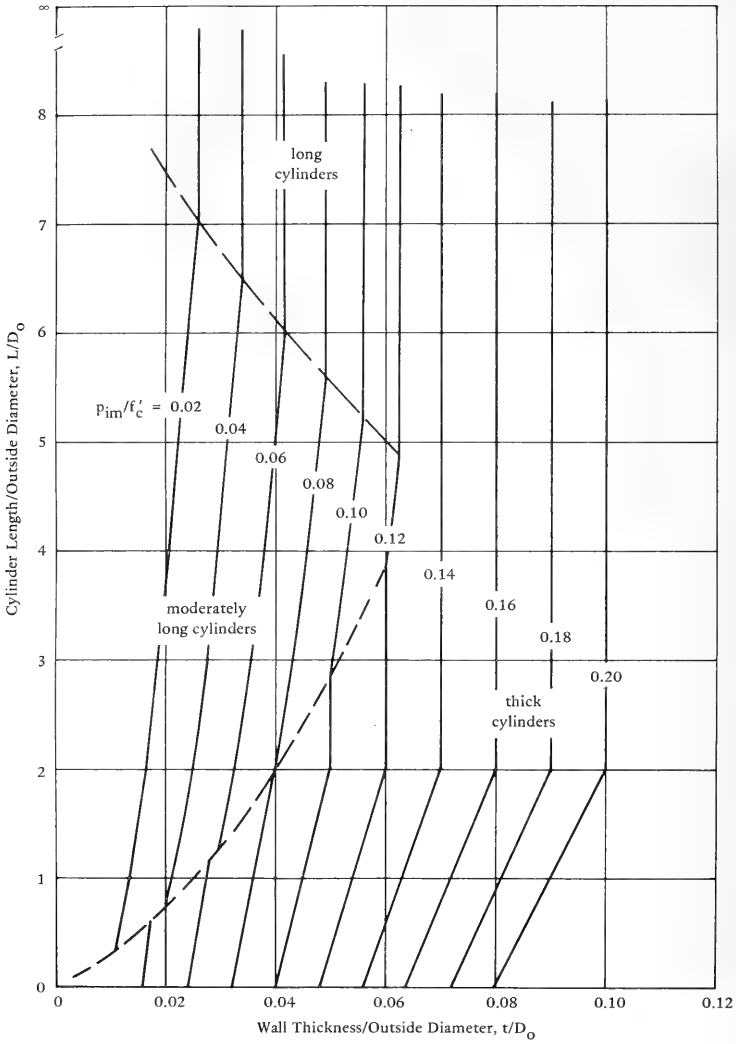

Figure 3. Design guide for predicting implosion of concrete cylinder structures.

Thin-Walled Cylinders

Table 1. Out-of-Roundness Parameters for 16-Inch OD Cylinders (Ref 2,4)

t/D_o	$\Delta t_{min}/t$	$\Delta R_i/t$	$\Delta R_o/t$
0.03[a]	0.12	0.12	0.12
0.06[b]	0.06	0.06	0.06
0.13[c]	0.03	0.03	0.03
0.19[c]	0.02	0.02	0.02

[a] Thin-walled cylinder.

[b] Border between thin- and thick-walled cylinder.

[c] Thick-walled cylinder.

Thin-walled cylinders are divided into two categories: moderately long cylinders and long cylinders. Moderately long cylinders are influenced by end-closures which restrain the cylinder from instability failure. Long cylinders are not influenced by end-closures and behave as infinitely long cylinders. In Reference 8, thin-walled cylinders included another category called short cylinders, but in this report the thick-walled cylinder category encompasses short cylinders (Figure 3).

The same approach used in Reference 8 is used herein. Donnell's equation is applied to moderately long cylinders and Bresse's equation to long cylinders. An empirical plasticity reduction factor, η, is used in both equations to account for inelastic behavior of concrete and specimen out-of-roundness. The new data permit an η relationship to σ_{im}/f'_c to be determined with far greater accuracy than previously.

Empirical η values were determined by calculating the elastic stress at buckling and dividing this stress into the experimental stress at implosion.

The elastic buckling stresses were calculated as follows:

Donnell's Equation

$$(\sigma_{im})_D = \frac{0.855\ E_i}{(1 - \nu^2)^{3/4}} \left(\frac{t}{R}\right)^{3/2} \frac{R}{L} \eta \qquad (4)$$

and

Bresse's Equation

$$(\sigma_{im})_B = \frac{E_i}{4(1 - \nu^2)} \left(\frac{t}{R}\right)^2 \eta \tag{5}$$

Using $\nu = 0.20$ and the approximation $R = D_o/2$, Donnell's equation becomes

$$(\sigma_{im})_D = \frac{1.25\ E_i\ \eta \left(\frac{t}{D_o}\right)^{1.5}}{L/D_o} \tag{7}$$

and Bresse's Equation

$$(\sigma_{im})_B = 1.04\ E_i\ \eta \left(\frac{t}{D_o}\right)^2 \tag{8}$$

The elastic condition exists when $\eta = 1$.

E_i was not measured for each specimen so an empirical relationship was developed to calculate its value. Figure 4 shows the experimental initial elastic moduli data as a function of compressive strength. The American Concrete Institute (ACI) expression for elastic moduli is shown for comparison along with the empirical expression:

$$E_i = 530\ f'_c \tag{9}$$

The empirical expression has the rational basis of being derived from the parabolic relationship for tangent modulus as follows:

$$E_t = \frac{2 f'_c}{\varepsilon_u} \sqrt{1 - \frac{\sigma}{f'_c}}$$

where E_t = tangent modulus

ε_u = ultimate strain (experimental average was 0.0025)

and the fitted condition of $\sigma = 0.56 f'_c$ when $E_i = E_t$.

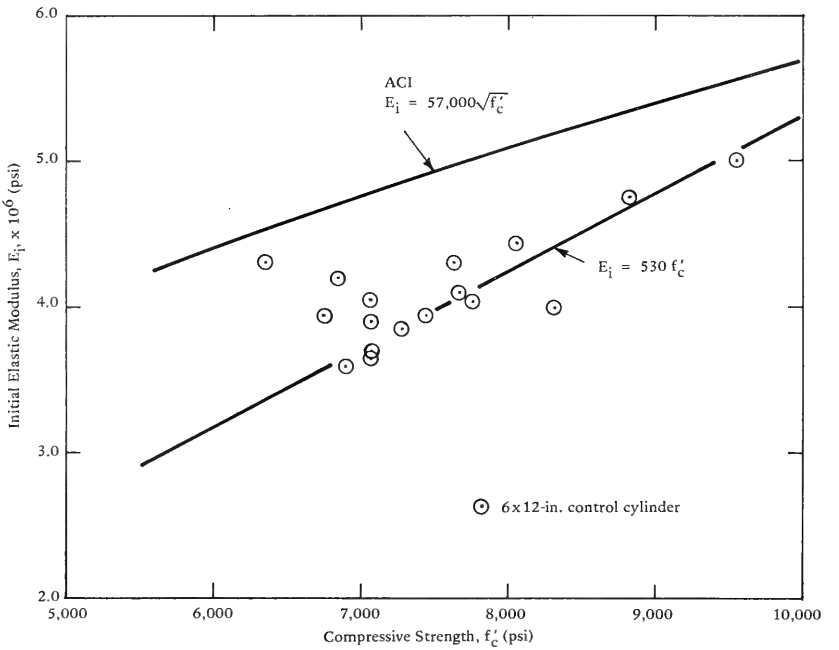

Figure 4. Relationship between E_i and f'_c.

Table 2. Plasticity Reduction Factors for 54-Inch OD Specimens

Specimen No.	Compressive Strength		Implosion Pressure, P_{im} (psi)	Initial Elastic Modulus,[b] $E_i \times 10^6$ (psi)	Average Wall Stress,[c] σ_{im} (psi)	$\frac{\sigma_{im}}{f'_c}$	Long Cylinders		Moderately Long Cylinders		Remarks
	f'_c (psi)	COV[a] (%)					Bresse's Stress,[d] $(\sigma_{im})_B$ (psi)	$\eta = \frac{\sigma_{im}}{(\sigma_{im})_B}$	Donnell's Stress,[e] $(\sigma_{im})_D$ (psi)	$\eta = \frac{\sigma_{im}}{(\sigma_{im})_D}$	
$t/D_o = 0.024$; Simple End-Supported; $L/D_o = 2.30$											
1-1	7,650	2.5	300	4.05	6,250	0.82	–	–	8,180	0.76	
1-2	8,310	1.8	329	4.40	6,850	0.82	–	–	8,890	0.77	
$t/D_o = 0.037$; Free End-Supported; $L/D_o = \infty$											
2-1	6,780	6.3	406	3.59	5,490	0.81	5,110	1.07	–	–	
2-2	8,690	4.8	400	4.61	5,410	0.62	6,560	0.82	–	–	
2-3	6,740	5.3	368	3.57	4,970	0.74	5,082	0.98	–	–	
2-4	7,820	3.1	330	4.14	4,460	0.57	5,890	0.76	–	–	Specimen defective
$t/D_o = 0.037$; Simple End-Supported; $L/D_o = 2.35$											
3-1	7,190	3.5	550	3.81	7,430	1.03	–	–	14,420	0.52	
3-2	6,830	9.2	575	3.62	7,770	1.14	–	–	13,700	0.57	
3-3	6,870	2.8	525	3.64	7,090	1.03	–	–	13,780	0.51	
3-4	8,170	7.1	342	4.33	4,620	0.57	–	–	16,390	0.28	Specimen defective
4-1	9,340	2.3	620	4.95	8,380	0.90	–	–	18,740	0.45	
4-2	7,310	9.8	590	3.87	7,970	1.09	–	–	14,650	0.55	
4-3	8,020	9.2	615	4.25	8,310	1.04	–	–	16,090	0.52	
$t/D_o = 0.063$; Free End-Supported; $L/D_o = \infty$											
5-1	7,990	2.2	1,078	4.23	8,060	1.07	17,460	0.46	–	–	
5-2	8,570	2.7	880	4.54	6,980	0.81	18,740	0.37	–	–	Specimen defective

[a] COV = Coefficient of Variation

[b] $E_i = 530\, f'_c$

[c] $\sigma_{im} = \dfrac{0.5\, P_{im}}{\dfrac{t}{D_o}}$

[d] $(\sigma_{im})_B = 1.04\, E_i \left(\dfrac{t}{D_o}\right)^2$

[e] $(\sigma_{im})_D = \dfrac{1.25\, E_i \left(\dfrac{t}{D_o}\right)^{3/2}}{\dfrac{L}{D_o}}$

Values of η are shown in Table 2. Table 3 shows the calculation of η values for the data from Reference 4.* All the data are shown in Figures 5 through 7. The fitted inelastic buckling curves of Figures 5 and 6 were transferred to Figure 8. From this representation of data, a design η curve was selected, which is applicable to both moderately long and long cylinders. The η expression is:

$$\eta = 1.65 - 1.25\left(\frac{\sigma_{im}}{f'_c}\right) \qquad 0.52 < \frac{\sigma_{im}}{f'_c} < 1 \qquad (10)$$

Gerard developed expressions to predict η for metallic structures (Ref 11), and these expressions, which can be applied to concrete, are shown graphically in Figure 9. The η curve from Reference 8 is also shown. Its empirical shape was defined by limited data where several specimens had low implosion pressures which are not in agreement with that of the new data. The new design η curve has a maximum increase of 35% over that of Reference 8. (For a structure of given geometry, comparative η values are obtained by a linear curve intersecting the origin and the η curves.)

*The values will be different than those given in Reference 8 because an assumption has been changed. Previously, the 16-inch OD specimens with hemisphere end-closures were assumed to be simply supported cylinders. This assumption was made at the time because the analysis of results would be conservative. Data were limited so conservatism was warranted. In this report, the 16-inch OD specimens, which had an $L/D_o = 4$, were assumed to be freely supported or, in other words, long cylinders.

Table 3. Plasticity Reduction Factors for 16-Inch OD Specimens (after Ref 4)

Specimen No.	Compressive Strength		Initial Elastic Modulus,[b] $E_i \times 10^6$ (psi)	Implosion Pressure, P_{im} (psi)	Average Wall Stress,[c] σ_{im} (psi)	$\frac{\sigma_{im}}{f'_c}$	Long Cylinders	
	f'_c (psi)	COV[a] (%)					Bresse's Stress,[d] $(\sigma_{im})_B$ (psi)	$\eta = \frac{\sigma_{im}}{(\sigma_{im})_B}$
$t/D_o = 0.031$; Free End-Supported; $L/D_o = \infty$								
1/2-10-N	10,700	2.3	4.50	376	6,020	0.56	4,570	1.32
1/2-10-G	10,900	5.0	4.54	349	5,580	0.51	4,610	1.21
1/2-6-N	5,420	3.9	3.00	203	3,250	0.60	3,050	1.07
1/2-6-G	5,760	2.6	2.60	214	3,424	0.59	2,640	1.30
$t/D_o = 0.063$; Free End-Supported; $L/D_o = \infty$								
1-10-N	10,700	1.5	4.50	1,110	8,880	0.83	18,280	0.49
1-10-G	10,480	1.4	4.32	1,103	8,820	0.84	17,550	0.50
1-6-G	6,620	1.9	3.20	543	4,340	0.66	13,000	0.33
1-6-N	5,920	5.8	3.10	530	4,240	0.72	12,590	0.34
$t/D_o = 0.125$; Free End-Supported; $L/D_o = \infty$								
2-10-G	9,840	3.2	3.90	2,335	9,340	0.95	63,370	0.15
2-10-N	9,950	4.7	4.24	2,455	9,820	0.99	68,900	0.14
2-6-N	6,080	3.0	3.29	1,387	5,550	0.91	53,460	0.10
2-6-G	6,060	2.3	3.36	1,447	5,780	0.96	54,600	0.11
$t/D_o = 0.188$; Free End-Supported; $L/D_o = \infty$								
3-10-G	10,350	2.8	4.10	3,755	10,010	0.97	149,910	0.07
3-10-N	10,800	2.2	4.60	4,107	10,950	1.01	168,190	0.07
3-6-N	7,000	3.0	2.94	2,405	6,410	0.92	107,490	0.06
3-6-G	6,200	2.2	3.11	1,980	5,280	0.85	113,710	0.05

[a] COV = Coefficient of Variation

[b] Actual value.

[c] $\sigma_{im} = \dfrac{0.5\, P_{im}}{\dfrac{t}{D_o}}$

[d] $(\sigma_{im})_B = 1.04\, E_i \left(\dfrac{t}{D_o}\right)^2$

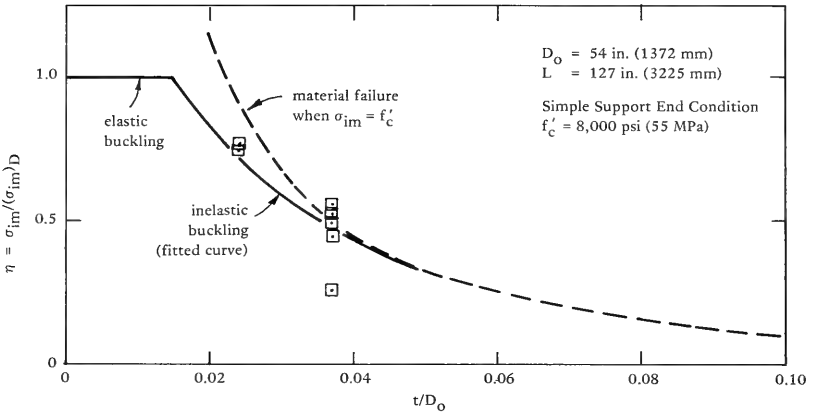

Figure 5. Implosion of moderately long cylinder specimens with D_o = 54 in. (1372 mm).

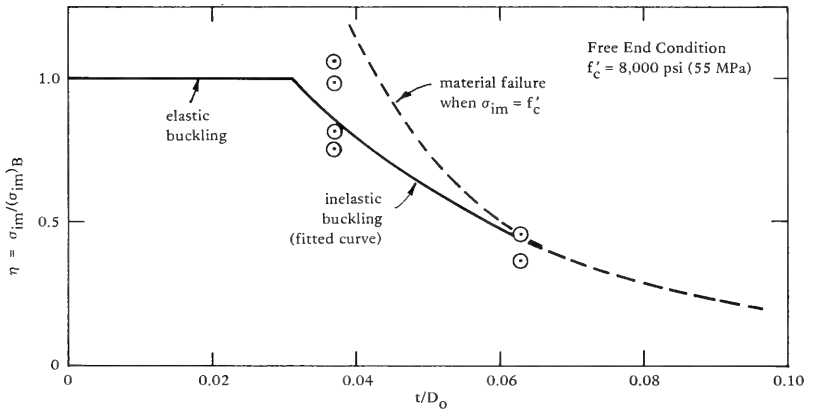

Figure 6. Implosion of long cylinder specimens with D_o = 54 in. (1372 mm).

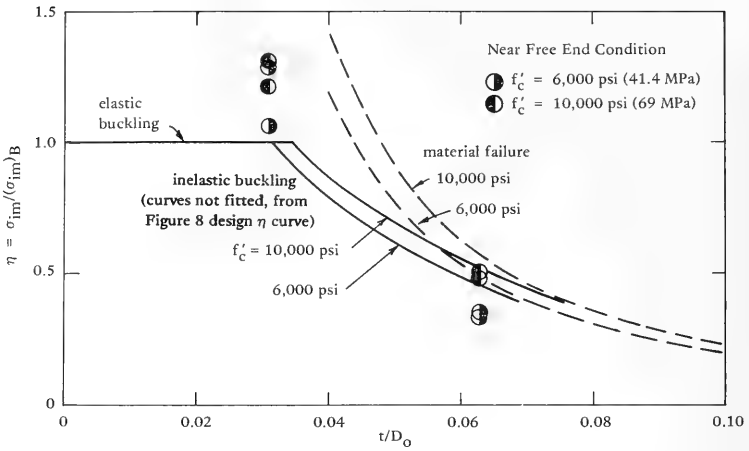

Figure 7. Implosion of long cylinder specimens with D_o = 16 in. (406 mm) (after Ref 4).

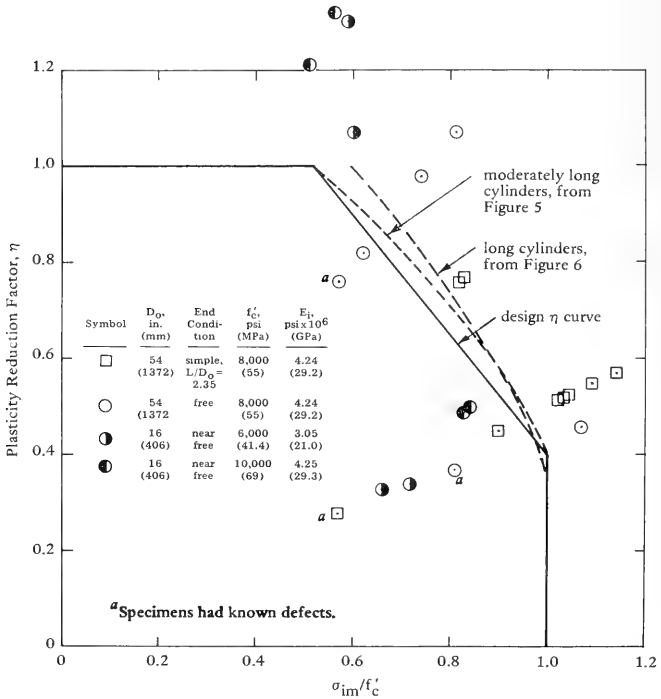

Figure 8. Plasticity reduction factor as a function of stress level in cylinder wall at implosion.

Gerard's Expressions:

Moderately Long Cylinders $$\eta = \left[\frac{1 - \nu_e^2}{1 - \nu^2}\right]^{3/4} \frac{E_s}{E} \left(\frac{E_t}{E_s}\right)^{1/4} \left(\frac{1}{4} + \frac{3}{4}\frac{E_t}{E_s}\right)^{1/2}$$

Long Cylinders $$\eta = \left[\frac{1 - \nu_e^2}{1 - \nu^2}\right] \frac{E_s}{E} \left(\frac{1}{4} + \frac{3}{4}\frac{E_t}{E_s}\right)$$

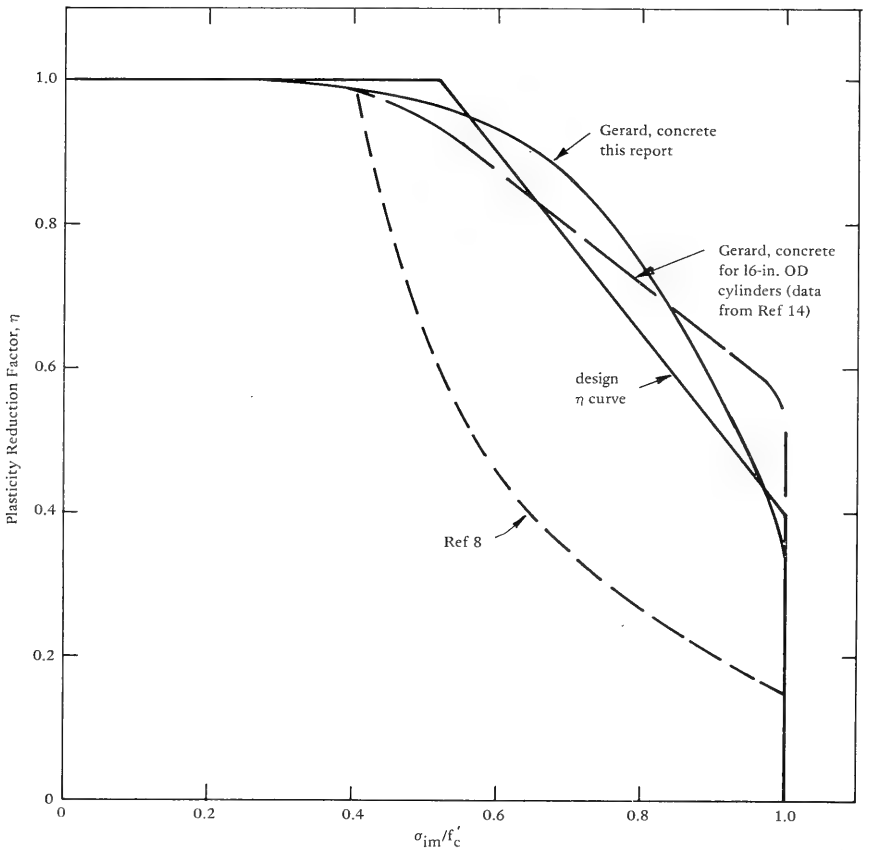

Figure 9. Comparison of various η versus σ_{im}/f_c' relationships.

Moderately Long Cylinders. The expressions to predict implosion pressure for moderately long cylinders are developed as follows.

Equations 9 and 10 are substituted into Equation 7 to yield:

$$\frac{\sigma_{im}}{f'_c} = \frac{1090\left(\frac{t}{D_o}\right)^{1.5}}{\frac{L}{D_o} + 830\left(\frac{t}{D_o}\right)^{1.5}} \tag{11}$$

The stress level at implosion, σ_{im}/f'_c, is calculated by knowing the geometry of the cylinder structure. The following conditions determine the next step:

(a) If $\sigma_{im}/f'_c > 1.0$, thick-wall analysis is used to predict implosion, Equation 3

(b) If $0.52 < \sigma_{im}/f'_c < 1.0$, then η is calculated by Equation 10

(c) If $\sigma_{im}/f'_c < 0.52$, then $\eta = 1.0$

If steps (b) or (c) control, the following expression, which was developed by substituting Equations 7 and 9 into Equation 1, predicts the implosion pressure.

$$P_{im} = \frac{1320\ \eta\ f'_c\left(\frac{t}{D_o}\right)^{2.5}}{L/D_o} \tag{12}$$

A design chart approach is given in Figure 3. Enter the chart with the structure's L/D_o and t/D_o ratio to determine the P_{im}/f'_c ratio. The structure is assumed to have a simple-support end condition.

For the case of fixed-support end condition, it has been shown analytically (Ref 12) that an increase in implosion strength on the order of 6% can be expected. The implosion pressure can be calculated for this case by using the equations presented herein and a reduced cylinder length of 0.85L.

Long Cylinders. The expressions to predict implosion pressure for long cylinders were developed as follows.

Equations 9 and 10 are substituted into Equation 8 to yield:

$$\frac{\sigma_{im}}{f'_c} = \frac{910\left(\frac{t}{D_o}\right)^2}{1 + 690\left(\frac{t}{D_o}\right)^2} \tag{13}$$

Once the stress level at implosion is calculated, the same conditions as for moderately long cylinders hold; that is:

(a) If $\sigma_{im}/f'_c > 1.0$, thick-wall analysis is used to predict implosion, Equation 3

(b) If $0.52 < \sigma_{im}/f'_c < 1.0$, then η is calculated by Equation 10

(c) If $\sigma_{im}/f'_c < 0.52$, then $\eta = 1.0$

If steps (b) or (c) control, the following expression, which was developed by substituting Equations 8 and 9 into Equation 1, predicts the implosion pressure:

$$P_{im} = 1100\,\eta\, f'_c \left(\frac{t}{D_o}\right)^3 \tag{14}$$

A design chart approach is given in Figure 3. Enter the chart with the structure's L/D_o and t/D_o ratio to determine the P_{im}/f'_c ratio.

Factor of Safety

Overall Factor of Safety. Up to this stage, the implosion pressure calculated by Equations 3, 12, and 14 (or from the design chart of Figure 3) is a short-term strength without any factors of safety incorporated. Different codes of practice have different approaches to assigning factors of safety. Without discussing the various methods, it can be stated that the overall factors of safety for concrete compression members range between 2.5 and 3.0.

This report recommends the same range. A structure whose intended purpose is to store liquid material might be designed with a 2.5 factor of safety; whereas, a structure for human occupancy should have a 3.0 factor of safety as a minimum.

The design approach in Reference 8 included a long-term loading factor, λ. Codes of practice typically recognize the long-term loading effect in the overall factor of safety without itemizing the effect. This report follows that practice. Results have recently been published on concrete spheres subjected to long-term hydrostatic loading (Ref 13) that have shown behavior similar to the known behavior of concrete in on-land compression members. This represents some assurance that following existing on-land practice is appropriate for in-ocean concrete.

Concrete Compressive Strength. The implosion pressure is directly related to the compressive strength of concrete, f'_c, at the time of failure. From available data (Ref 13), it appears that the strength development of concrete in the ocean is different than that of the standard fog-cure condition.

The results from Reference 13 are summarized herein.

If saturation of concrete is assumed to occur, then the following interim guide can be used for strength gain with age. The initial 28-day fog-cured strength should be reduced by 10% to account for saturation effects. Subsequent increases of in-situ strength with time may depend on the depth at which the concrete is located. Depth is important because it can influence the degree of saturation. At present, data are available at depths of a few thousand feet. In such cases, the strength increase relative to the 28-day fog-cured strength appears to be nil at 1 year, 5% at 2 years, and 15% at 5 years. These values of strength-increase-with-age are different from those generally accepted (Ref 14) for on-land concrete of 20% at 6 months and 24% at 12 months.

For cases where the concrete is at a depth of a few hundred feet, it is hard to estimate the strength gain behavior. First, it is unknown how much of the wall thickness will become saturated. It could take months for several feet of thickness to become saturated. If the interior of the structure were to be at a relative humidity of less than 100%, the concrete would never become saturated. However, some of the concrete would be saturated near the outside wall, and that portion would exhibit a strength different from that not saturated. For the saturated concrete the compressive strength should be reduced by 10% to account for saturation effects; then it is probably reasonable to permit a strength increase relative to the 28-day fog-cured strength of nil at 6 months and 5% at 12 months.

Effect of Reinforcement. The experimental specimens were unreinforced concrete, whereas any full-scale structure would be reinforced concrete. The reinforcement certainly contributes to stiffening of the wall during bending caused by out-of-roundness. However, under ultimate conditions the contribution of the reinforcement is not easily assessed.

It is recommended that the procedures stated in various codes of practice be adapted. For compression members the effect of reinforcement is permitted to contribute to the ultimate capacity of the member as long as the reinforcement is tied against lateral movement as in a column. If the compression reinforcement is not tied, then the member is designed as unreinforced concrete.

Out-of-Roundness. The design chart in Figure 3 is based on empirical data and, therefore, contains an inherent out-of-roundness allowance. This allowance for thick-walled cylinders is given in Table 1. The thin-walled cylinder test specimens were studied in detail for out-of-roundness, and Table B-2 in Appendix B (pg 51) presents a digest of their out-of-roundness. A structure having geometric tolerances equal to or less than the test specimens will be safely designed using Figure 3. Conventional construction practices should encounter few problems in matching the geometric tolerances of the test specimens.

It is recommended that, once a structure is sized-out by Figure 3 and meets its other design requirements, a detailed finite element analysis be conducted. The analysis should assume a realistic out-of-round geometry and model the inelastic behavior of concrete materials.

SUMMARY

The updated design guides represent some significant changes compared to the guides presented in Reference 8. The design approach for thick-walled cylinders was made comparable to that for thick-walled spheres by using an average wall stress equation with an empirical strength factor, k_c. Thin-walled cylinders used the same design approach as described in Reference 8; however, new experimental results from 15 relatively large-scale specimens permitted a more accurate development of an empirical plasticity reduction factor, η.

The effect of test specimen out-of-roundness is included in the empirically derived portions of the guides so use of the guides implicitly assumes out-of-roundness of similar magnitude for the new structure. This is a safe assumption because out-of-roundness criteria as given in Table 1 and Table B-2 are lenient for large structures (in other words, large structures should have better geometry control than the test specimens).

Figure 3 is a design chart to predict implosion for thick- and thin-walled concrete cylinder structures. A feature of the chart is its simplicity. By knowing the t/D_o and L/D_o ratio of the structure, the implosion strength in terms of P_{im}/f'_c can be determined. Implosion pressure, P_{im}, is calculated by assigning an f'_c to the concrete. A factor of safety is not included in the predicted implosion pressure.

The design chart has application in sizing-out a structure for a given depth. Advanced design techniques must be used to complete a final design, but these techniques need to start from near-final dimensions. This report provides the design charts to quickly determine the near-final dimensions.

CONCLUSIONS

1. Failure of concrete cylindrical structures under hydrostatic loading can be described by one of three equations: an average wall stress equation applies to thick-walled cylinders; Donnell's equation to moderately long, thin-walled cylinders; and Bresse's equation to long thin-walled cylinders. An empirical parameter was used in each equation to obtain agreement between the experimental results and theoretical expression.

2. The finite element analysis method with a constitutive material model predicted the implosion strength and structural displacement

behavior of the test specimens with good accuracy (Appendix B). Figure 3, which is the design chart for implosion, is within 10% accuracy of the finite element method predictions.

3. The design chart of Figure 3 can be applied for quickly determining the implosion strength for a concrete cylinder structure of given dimensions.

ACKNOWLEDGMENTS

EXXON Production Research Company is acknowledged for their co-sponsorship of the thin-walled cylinder test program.

At CEL, Roy S. Highberg and Philip C. Zubiate are recognized for conducting tests on both the thin- and thick-walled cylinder specimens. Other participants were Joseph F. Wadsworth, Joseph Graham, Gene McMahan, and Michael Hanks.

REFERENCES

1. Civil Engineering Laboratory. Technical Report R-517: Behavior of spherical concrete hulls under hydrostatic loading, Part I. Exploratory Investigation, by J. D. Stachiw and K. O. Gray. Port Hueneme, Calif., Mar 1967. (AD 649290)

2. _____. Technical Report R-696: Influence of length-to-diameter ratio on the behavior of concrete cylindrical hulls under hydrostatic loading, by H. H. Haynes and R. J. Ross. Port Hueneme, Calif., Sep 1970. (AD 713088)

3. _____. Technical Report R-740: Influence of end-closure stiffness on behavior of concrete cylindrical hulls subjected to hydrostatic loading, by L. F. Kahn. Port Hueneme, Calif., Oct 1971. (AD 732363)

4. _____. Technical Report R-790: Influence of compressive strength and wall thickness on behavior of concrete cylindrical hulls under hydrostatic loading, by N. D. Albertsen. Port Hueneme, Calif., Jun 1973. (AD 764054)

5. H. H. Haynes. "Research and development of deep-submergence concrete," in Proceedings of Federation Internationale de la Precontrainte (FIP) Symposium on Concrete Sea Structures. Tblisi, USSR, Sep 1972, pp 180-185.

6. H. H. Haynes and B. A. Nordby. "Concrete cylinder structures under hydrostatic loading," in Proceedings, American Concrete Institute, vol 73, no. 2, Feb 1976, pp 87-96.

7. H. H. Haynes. "Implosion criteria and behavior considerations for concrete deep submergence vessels," in Proceedings of Conference on Concrete Ships and Floating Structures, University of California, Berkeley, Calif., Sep 1975, pp 77-92.

8. Civil Engineering Laboratory. Handbook for design of undersea, pressure-resistant concrete structures, by H. H. Haynes. Port Hueneme, Calif., Sep 1976, p 35.

9. _____. Technical Report R-817: Seafloor construction experiment, SEACON I - An integrated evaluation of seafloor construction equipment and techniques, by T. Kretschmer et al. Port Hueneme, Calif., Feb 1975.

10. H. Kupfer, H. K. Hilsdorf, and H. Rusch. "Behavior of Concrete Under Biaxial Stresses," in Proceedings, American Concrete Institute, vol 66, no. 8, Aug 1969, pp 656-666.

11. G. Gerard. "Plastic stability theory of thin shells," Journal of the Aeronautical Sciences, vol 24, no. 4, Apr 1957, pp 269-274.

12. O. Olsen. "Implosion analysis of concrete cylinders under hydrostatic pressure," in Proceedings, American Concrete Institute, vol 75, no. 3, Mar 1978, pp 82-85.

13. Civil Engineering Laboratory. Technical Report R-869: Long-term deep-ocean test of concrete spherical structures - Results after 6 years, by H. H. Haynes. Port Hueneme, Calif., Jan 1979, p. 48.

14. A. M. Neville. Properties of concrete, 2nd Ed., New York, N.Y., Pitman Publishing, 1973, p. 259.

15. Civil Engineering Laboratory. Technical Report R-588: Behavior of spherical concrete hulls under hydrostatic loading, Part III - Relationship between thickness-to-diameter ratio and critical pressures, strains, and water permeability rates," by J. O. Stachiw and K. Mack. Port Hueneme, Calif., Jun 1968 (AD 8354926).

16. _____. Technical Memorandum M-44-76-4: Results of concrete cylinder implosion test program, by Harvey H. Haynes and Roy S. Highberg. Port Hueneme, Calif., Apr 1976, p. 391.

17. _____. Technical Note N-1367: Adhesives for use underwater, by R. W. Drisko, J. B. Crilly, and R. M. Staples. Port Hueneme, Calif., Dec 1974.

18. _____. Technical Note N-1173: Evaluation of eight epoxy adhesives for bonding concrete and microconcrete structural components exposed to room and hydrostatic pressure conditions, by T. Roe, A. F. Curry, and P. C. Zubiate. Port Hueneme, Calif., Jul 1971.

19. S. P. Timoshenko and J. M. Gere. Theory of elastic stability, 2nd Ed. New York, N.Y., McGraw-Hill, 1961, p. 295.

20. Purdue University. CE-STR-78-2: Analysis of concrete cylinder structures under hydrostatic loading, by W. F. Chen, H. Suzuki, and T. Y. Chang. West Lafayette, Ind., Apr 1978, pp 157.

21. A. C. T. Chen and W. F. Chen. "Constitutive relations for concrete," Journal of the Engineering Mechanics Division, ASCE, vol 101, no. EM4, Aug 1975, pp 465-481.

22. W. F. Chen. Limit analysis and soil plasticity. Amsterdam, The Netherlands, Elsevier, 1975.

23. University of Akron, Department of Civil Engineering. Report No. SE 76-3: NFAP - A Nonlinear Finite Element Analysis Program, by T. Y. Chang, and S. Pinchaktan. Akron, Ohio, Oct 1976.

24. Energy Research and Development Agency. Report No. C00-2682-7: Extended NONSAP Program for OTEC Structural Systems, by T.Y. Chang and W. F. Chen. Washington, D.C., 1976.

25. University of California, Department of Civil Engineering. SESM Report No. 73-3: NONSAP - A structural analysis program for static and dynamic response of nonlinear systems, by K. J. Bathe, E. L. Wilson, and R. H. Iding. Berkeley, Calif., 1974.

26. H. H. Haynes and L. F. Kahn. "Undersea Concrete Spherical Structures," Proceedings, American Concrete Institute, vol 70, no. 5, May 1973, pp 337-340.

Appendix A

THICK-WALLED CYLINDER TESTS

SPECIMEN DESCRIPTION

The SEACON I structure (Figures A-1 and A-2) was assembled from three precast, reinforced concrete sections. The straight cylinder section, 10.1-foot (3.08-m) OD by 10-foot (3.05-m) length by 9.5-inch (241-mm) wall thickness, was fabricated by United Concrete Pipe Corporation. The concrete hemisphere end-closures, 10.1-foot (3.08-m) OD by 9.5-inch (241-mm) wall thickness, were fabricated in-house. Tolerances on the sections conformed to concrete pipe standards: ID not to exceed ±0.75 in. (19 mm) or wall thickness not to exceed -0.5 in. (13 mm).

Steel reinforcement of 0.70% by area was used in both the hoop and axial direction. Reinforcing bars of 0.50 inch (15 mm) diameter were employed throughout the structure. A double circular reinforcement cage was fabricated for each precast section; the concrete cover on the outside and inside reinforcing cage was 1 inch (25 mm). For the cylinder section, hoop rebars had a center-to-center spacing of 6 inches, and axial rebars had a spacing of 27.25 inches (692 mm) and 31.25 inches (794 mm) for the inside and outside cages, respectively.

The hemispherical end-closures were bonded to the cylinder section with an epoxy adhesive; no other attachment besides the epoxy bond was employed. The gap between the mating surfaces of the hemisphere and the cylinder was less than 0.13 in. (3 mm) for 75% of the contact area. Prior to epoxy bonding, the concrete surfaces were sandblasted and washed with acetone.

Figure A-1. SEACON structure prepared for ocean test to implosion.

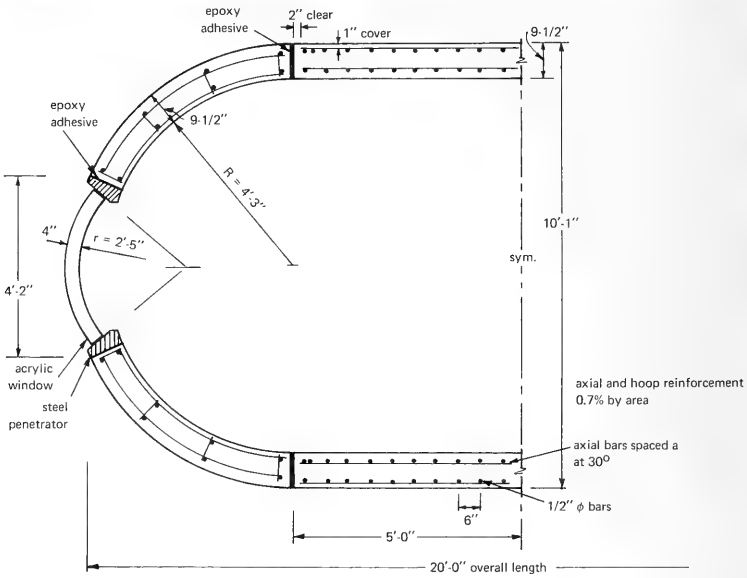

Figure A-2. Details of SEACON structure.

A large hull penetration, major diameter of 50.25 in. (1275 mm) and minor diameter of 42.4 in. (1075 mm), was located at the apex of each hemisphere. This penetration size was equivalent to 40% of the hemisphere diameter. The design philosophy for the penetrator was to make it stiffer than the concrete material it replaced so that the hemisphere was "unaware" of the large hole. The steel penetrator was epoxy-bonded to the concrete, using the surface preparation method described for the joint.

During the 10-month seafloor construction experiment, an acrylic window assembly was used in one penetrator and a hatch assembly in the other penetrator. The window and hatch were subsequently replaced with steel plates for the implosion test.

Six penetrations, major diameter of 6 inches (152 mm) and minor diameter of 5 inches (127 mm), were included in one of the hemispheres; these penetrations were part of a seal and gasket study.

Two smaller penetrations, major diameter of 4.5 inches (114 mm) and minor diameter of 4.0 inches (102 mm), were also included near the center of the cylinder section to accommodate pressure relief valves.

For the implosion test, three of the small hemisphere penetrators were modified for electrical feed-throughs and pressure ports. The two cylinder penetrations were sealed.

Additional irregularities in the concrete wall included five feed-through boxes for strain gages mounted on reinforcing bars. These boxes were located on the interior wall and measured 2.5 inches (64 mm) deep by 4 inches (102 mm) in diameter. In these areas the local wall thickness was reduced to 7 inches (178 mm).

Prior to the implosion test, fifteen 3.25-in. (83-mm) diameter cores were drilled from the wall at various locations around the cylinder. Steel plugs were epoxied in the core holes.

During original assembly, the exterior of the concrete structure was coated with a phenolic waterproofing system. After lightly sand-blasting the concrete, a primer and topcoat (Phenoline no. 300) were

sprayed onto the concrete. Many air pockets were not coated; approximately one pinhole per 2 in.^{2} (1300 mm^2) existed in the final waterproofing coating.

The concrete structure was instrumented with a total of 40 electrical resistance strain gages to monitor hull response under long-term loading. Half of the gages were placed diametrically opposed to each other on the structure. The data were stored on magnetic tape inside the structure and were recovered when the structure was retrieved after 10 months.

The concrete material for the cylinder portion of the structure consisted of portland cement type II, sand, and coarse aggregate in the proportions of 1.0:1.4:2.5 by weight, respectively. The water-to-cement ratio was 0.40 by weight, and a water-reducing admixture was used; the slump was 1.25 inch (32 mm). The average compressive strength at 28 days of the 6-inch (152-mm) diameter by 12-inch (305-mm) long control cylinders was 7,800 psi (53.8 MPa).

Mix designs of different proportions were used for the hemispheres: cement-to-sand-to-coarse-aggregate ratio of 1.0:1.95:2.3 by weight; water-to-cement ratio of 0.38 by weight; and a water-reducing admixture. Slump was again 1.25 inch (32 mm). The average compressive strength at 28 days was 8,170 psi (56.3 MPa).

Of the 15 cores taken from the cylinder wall just prior to the implosion test, 7 were subsequently cut into 3.25-in. (83-mm) diameter by 6-in. (152-mm) long cylinders, which were tested under uniaxial compression. Compressive strengths of the cores and from a number of 6x12-inch (152x305-mm) control cylinders at various ages are presented in Table A-1.

Three of the core specimens were instrumented with strain gages to obtain stress-strain data for the concrete. Curves of this relationship up to about 90% of the compressive strength are shown in Figure A-3. The secant modulus of elasticity to about 40% of f'_c was 4.4×10^6 psi (30.4 GPa), and Poisson's ratio was 0.20.

Table A-1. Summary of Concrete Compressive Strengths for the Seacon Structure

Specimens				Age of Concrete (days)	Compressive Strength (psi)
Type	Size (in.)	Number	Curing Conditions[a]		
cast	6 x 12	6	field	28	7,800
cast	6 x 12	2	fog	96	7,070
cast	6 x 12	2	field	96	8,550
cast	6 x 12	3	fog	294	9,190
cast	6 x 12	3	field	294	9,710
cast	6 x 12	6	fog	608	8,710
cast	6 x 12	3	fog and ocean[b]	608	8,620
cast	6 x 12	3	field and ocean[c]	608	8,370
core	3.25 x 6	7	part of structure[d]	2,128	10,470

[a]Curing of all cylinders for the first 28 days was 2 days steam, 7 days water tank, and 19 days field.

[b]After first 28 days, curing was 270 days fog room and 302 days on seafloor at 600 feet.

[c]After first 28 days, curing was 270 days field and 302 days on seafloor at 600 feet.

[d]Structure was field-cured on land for 298 days, on the seafloor for 302 days, and then field-cured on land for 1,528 days.

As shown in Figure A-1, the concrete cylinder structure was mounted in a steel framework and fitted with a ballast tank. The in-air weight of the cylinder was 85,000 pounds (38.5 Mg), and the concrete-steel structure weighed 102,000 pounds (46.3 Mg). The positive buoyancy of the concrete hull was 12,000 pounds (5.4 Mg), and when ballasted the concrete-steel structure weighed 6,800 pounds (3.1 Mg) negative in water.

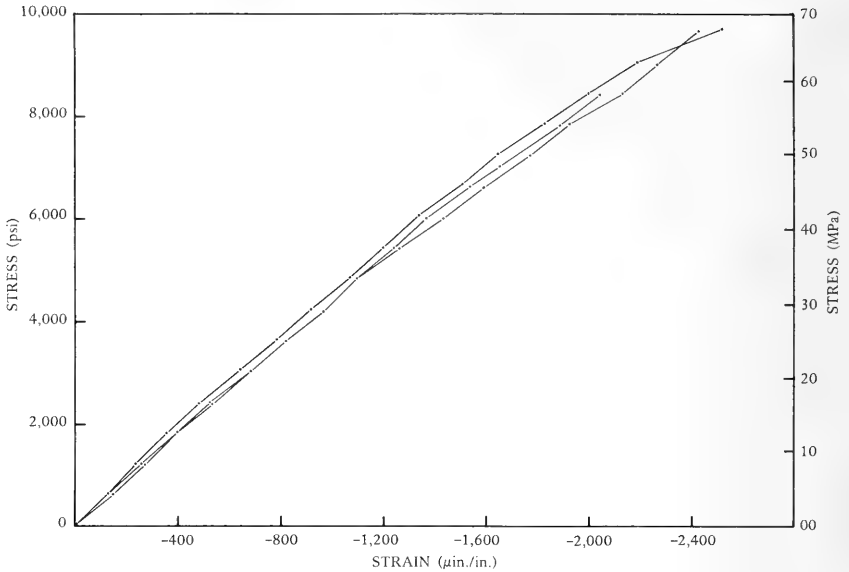

Figure A-3. Stress-strain curves from 3.25-in. diam x 6-in. long cores.

TEST RESULTS

Long-Term Test at 600 Feet

Strain Behavior. The initial strain response of the structure on being lowered to 600 feet (180 m) showed an average strain of 380 μin./in. in the hoop direction and 170 μin./in. in the axial direction (Ref 9). From previous work (Refs 2, 3 and 4), it was anticipated that this low level of loading should not have produced any detectable strain variation along the length of the cylinder section due to the discontinuity of the cylinder/end-closure joint. The actual strains showed this to be true.

The concrete was under sustained stress of 1,700 psi in the hoop direction and 920 psi in the axial direction for 302 days. The average total creep strain in the hoop and axial direction was 130 and 80 μin./in., respectively; these values represent a 34% and 47% increase, respectively, over the short-term strain (not unusual for concrete). The data gave no indication that the creep strain was nearing termination.

The large penetration had little effect on the behavior of the hemisphere. Again, the low stress level in the concrete might not have been sufficient to produce a noticeable strain rise at the penetration. In any event, it was significant that the penetrator, equivalent to 40% of the structure's diameter, did not produce a harmful effect on the structure.

Watertightness. Upon retrieval of the cylinder from the 600-foot (180-meter) depth after 10 months, the interior of the structure was free from water that permeated the concrete walls. There was no evidence of condensation, or even dampness, on the interior concrete walls.*

Results from long-term loading of concrete spheres in the ocean (Ref 13) confirm this finding of watertightness. The 66-inch (1076-mm) OD spheres had a wall thickness of 4.12 inches (105 mm) and were located at depths that ranged from 2,000 to 5,000 feet (600 to 1500 meters). Some of the sphere exteriors were coated identical to the SEACON structure and showed no water on the interior after 6 years in the ocean.

Implosion Test

Depth at Implosion. The depth of implosion for the structure was 4,700 feet (1430 m).

*Three quarts of water were found inside the structure due to a leak in a check valve in one of the small penetrators under investigation.

The means of determining the depth of implosion was not as straightforward as originally planned. Pressure transducers were installed on the hull, but these were inoperative at the time of implosion. During launching of the structure, which was off the stern of an offshore work vessel, a small hull penetration became damaged and resulted in a leak of about 25 gallons (95 liters) of seawater per minute. The weight of the structure increased until a safety link in the lowering line parted, which occurred at a depth of 2,900 feet (884 meters), as recorded by the pressure transducers. From this depth on, the structure free-fell through the water column until implosion occurred.

Data from acoustic depth-recording instrumentation were continuously being recorded on tape during this sequence of events. The noise generated by the implosion of the structure was also recorded. This signal had a rather long duration and showed that implosion could have occurred at a depth between 4,500 feet (1370 meters) and 4,700 feet (1430 meters). Seafloor depth was 4,700 feet (1430 meters).

It was known from data on tape that the time between the start of free-fall and implosion was 160 seconds. By analytically bracketing the free-fall velocity of the structure between 11.2 ft/sec (3.4 m/sec) and 12.5 ft/sec (3.8 m/sec), it was calculated that the structure free-fell between 1,790 feet (546 meters) and 2,000 feet (610 meters). Adding these numbers to 2,900 feet (884 meters) gave the total depth range as 4,690 feet (1430 meters) to 4,900 feet (1494 meters). Hence, it was apparent that the structure hit the seafloor at a depth of 4,700 feet (1430 meters) before imploding.

A manned submersible inspection by the Navy's Sea Cliff was conducted in 1978 to determine whether the structure imploded after impacting the seafloor. The tight grouping of fragments confirmed that the structure hit the seafloor first. If the structure had imploded during free-fall descent, the fragments would have been scattered. The inspection also confirmed that the cylinder section imploded rather

than that one of the hemispheres or a penetrator failed. The cylinder section was heavily fragmented while the hemispheres were rather recognizable.

There were no means of estimating whether the structure imploded immediately upon hitting the bottom or remained on the bottom for a time before imploding. In any event, 4,700 feet (1430 meters) is a conservative (or minimum) implosion depth.

It should be mentioned that the structure was instrumented for strain readings during the implosion test. The damaged penetrator, however, was also the electrical feed-through for strain-gage wires; therefore strain readings were not recorded during the test.

Discussion of Implosion Strength. The effect of hull stress rate, due to free-fall velocity, was not considered a significant parameter on implosion strength when compared to previously tested cylinder models. For a free-fall velocity of 11.2 ft/sec (3.4 m/sec), the hoop stresses in the hull increased at a rate of 1,900 psi/min (13.1 MPa/min). Previous cylinder models with geometry equivalent to that of the SEACON structure had hoop stress rates about 700 psi/min (9.8 MPa/min). This difference in stress rate would have an insignificant effect on implosion strength.

Pressure buildup inside the structure was minimal during the entire test. At the 2,900-foot (880-meter) depth it was known that 13,000 pounds (5.9 Mg) of seawater leaked to the interior. This filled about one-quarter of the interior volume. By the time implosion occurred, the interior pressure would not have exceeded 5 psi (34 KPa) over atmospheric. The exterior pressure at implosion was 2,100 psi (14.5 MPa).

The implosion strength of the SEACON hull was

$$\frac{P_{im}}{f'_c} = \frac{2{,}100 \text{ psi}}{10{,}407 \text{ psi}} = 0.200$$

The compressive strength, f'_c, was obtained from 3.25x6-inch (83x152-mm) core specimens. The strength of the cores was assumed equal to that of 6x12-inch (152x305-mm) cast specimens. The smaller size of the core specimens would cause a higher strength relative to 6x12-inch cylinders; however, this strength increase would be offset by the effect of drilling which causes a strength decrease.

With the use of the average wall stress approach as expressed in Equation 3, the material strength factor was calculated as:

$$k_c = \frac{(P_{im}/f'_c)}{2(t/D_o)} = \frac{0.200}{2(9.5/121)} = 1.27$$

This factor is shown in Figure 1 for the SEACON hull which had an $L/D_o = 1.0$.

The effect of steel reinforcement on the implosion strength of the structure could not be determined from this test. If the reinforcement was considered effective, then the total wall thickness from transformed sections would be 10.07 inches. This represents an increase of 6% over that of the actual wall thickness, which should cause an equivalent increase in the implosion pressure. This single test could not determine such a small percentage difference in strength.

FINDINGS

1. The implosion depth for the SEACON structure was 4,700 feet (1430 meters). Core specimens 3.25 inches (83 mm) in diameter by 6 inches (152 mm) long taken from the hull gave the uniaxial compressive strength of 10,470 psi (72.2 MPa).

2. With the use of the average wall stress equation, the material strength factor, k_c, was 1.27; the wall stress at implosion was 13,300 psi.

Appendix B

THIN-WALLED CYLINDER TESTS

SCOPE

A total of 15 unreinforced concrete cylinder specimens were tested under hydrostatic loading. The dimensions of the specimens were a constant outside diameter, D_o, of 54 inches (1372 mm), overall length of 134 inches (3400 mm), and wall thicknesses, t, of 1.31, 1.97, or 3.39 inches (33, 50, or 86 mm). The wall-thickness-to-outside-diameter, t/D_o, ratios were 0.024, 0.037, and 0.063, respectively. Two different types of boundary conditions were used: a simply supported and a free end-condition. Twelve of the specimens were tested under short-term hydrostatic loading where the pressure was increased until implosion; the remaining three specimens were subjected to long-term loading.

Structural behavior was recorded by measuring radial displacements around the entire circumference of the cylinder wall at various locations along the length. Deflected cross-sectional shapes were plotted from which the following data could be determined:

(a) Initial deviations from circularity

(b) Radial displacements due to membrane shell action and bending

(c) Location of the worst flat-spot and determination of maximum radial displacement

(d) The number of buckle lobes at implosion

Attempts were made to obtain strain data but difficulties were encountered in applying gages to wet concrete.

Inspection of failed specimens and fragments of concrete from the failure zones yielded data on the deflected shape of the structure and size of the failure hole.

A detailed presentation of specimen geometry and test results is given in Reference 16. This report summarizes portions of those data.

SPECIMEN FABRICATION

Casting

The specimens were cast monolithically in steel molds. The same outer mold was used for all specimens, but different inner molds were used to change the wall thickness. The inner molds were built to fold inward so that the diameter became smaller for removal from inside of the concrete cylinder. The inner and outer molds were spaced on the bottom by a ring and on the top by a spreader bar.

Concrete was placed in the molds by free falling from a dome distribution plate. When the form was vibrated, the concrete flowed to the edges of the dome and fell into the mold. By this technique, the concrete was evenly distributed around the circumference.

Approximately 20 hours after casting, the mold was removed from the concrete (Figure B-1). All specimens were wrapped in wet burlap and then in polyethylene film. They were subsequently moved to a sheltered storage area where a water drip system kept the burlap wet.

Figure B-1. Cylinder specimen being removed from mold.

Figure B-2. Specimen partly assembled inside polyethylene tent.

The specimens were moist-cured in this manner until assembled for test. During assembly (Figure B-2) a tent of polyethylene film was used to maintain a high relative humidity environment around the specimen to minimize shrinkage cracking. Keeping the cylinder in the moist environment assured the test conductors that the concrete was in a "wet" condition at the time of the implosion test.

Assembly

The procedure to assemble a specimen for test (Figure B-3) began by placing the cylinder on the bottom end-closure, which was a flat steel plate. The top end-closure was a steel ring. The top and bottom closures were held together by eight chains, post-tensioned to precompress the concrete by 20 psi (0.14 MPa) when the structure was submerged in water in the pressure vessel.

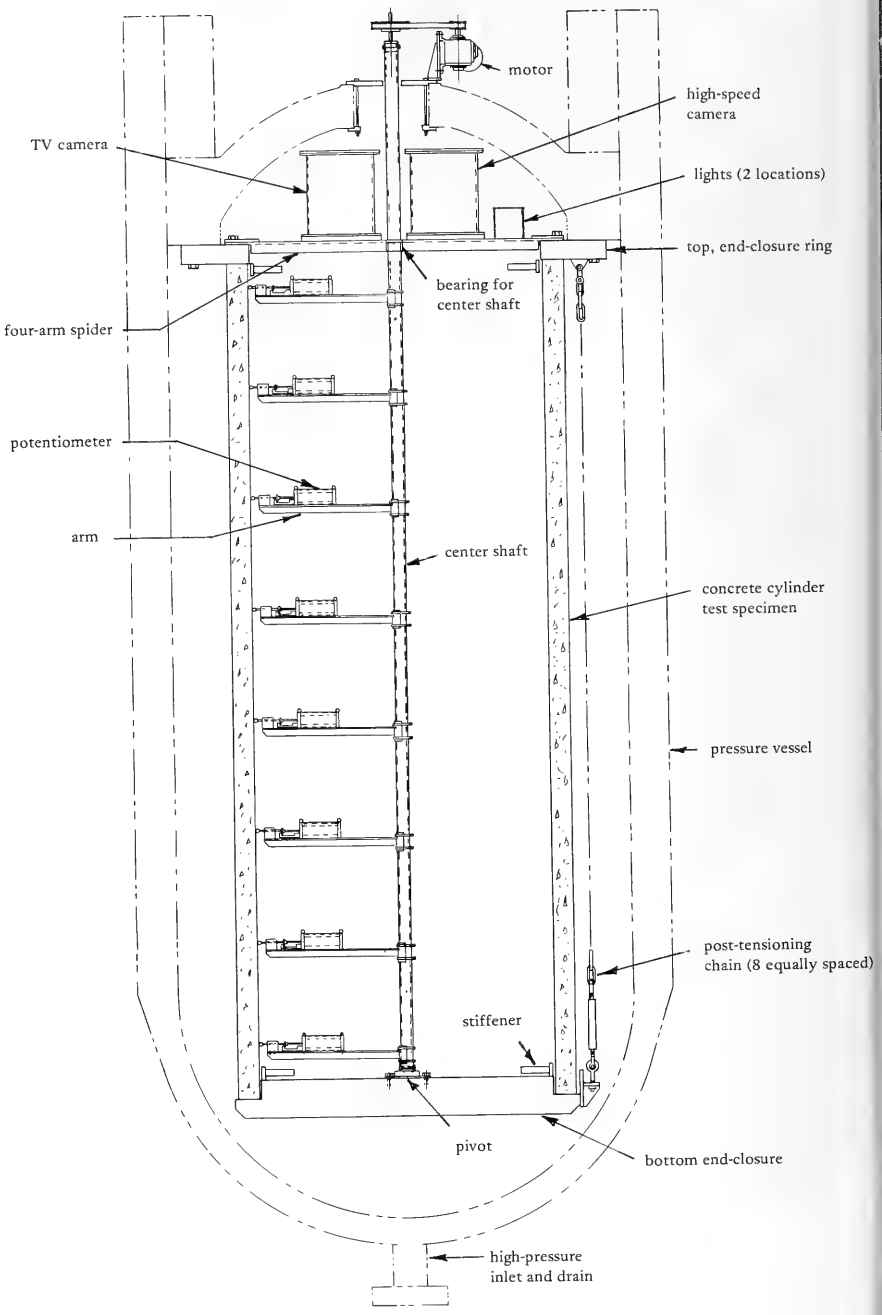

Figure B-3. Cross section of specimen, showing test setup.

For the simply supported end-condition (Figure B-4) epoxy adhesive was placed between the concrete and steel ends to correct for unevenness at the mating faces. Later, steel stiffeners were placed in the interior at the top and bottom, and expansive-cement grout was packed between the stiffeners and the concrete wall. For the free support end-condition (Figure B-4), a 1/8-in. (3-mm) neoprene rubber gasket was placed between the steel and concrete. A thin layer of epoxy adhesive or quick-setting gypsum was used between the concrete and the neoprene gasket.

When the specimen was assembled to the stage where the center shaft was centered at the top and bottom, radius measurements were taken using the following procedure. An arm off the center shaft had a scribe marker mounted to it. A fixed position table was placed beneath the arm, so when the center shaft was rotated, a circle was scribed on the table. The radius of this circle, r', was measured after the table was removed from the specimen. At the circumferences of 0, 90, 180, and 270 degrees, the distance from the scribe to the wall, r", was measured using a steel rule accurate to 0.01-inch (0.25-mm). By adding r' and r", the inside radius of the specimen was obtained at the circumference locations. Deviations in radius around the circumference were obtained from deflectometer data, so by using the deflectometer data and the measured radius data, average radius values for the specimens were determined.

Instrumentation

Instrumentation of the specimens consisted of mounting a deflectometer system to measure radial displacements, applying strain gages (to some specimens), installing a television camera, and installing a high-speed motion picture camera. These systems are described below.

Deflectometer. The measuring device of the deflectometer system was a potentiometer (linear position transducer) which had a maximum displacement of ±0.650 in. (16.51 mm) and a measurement accuracy of

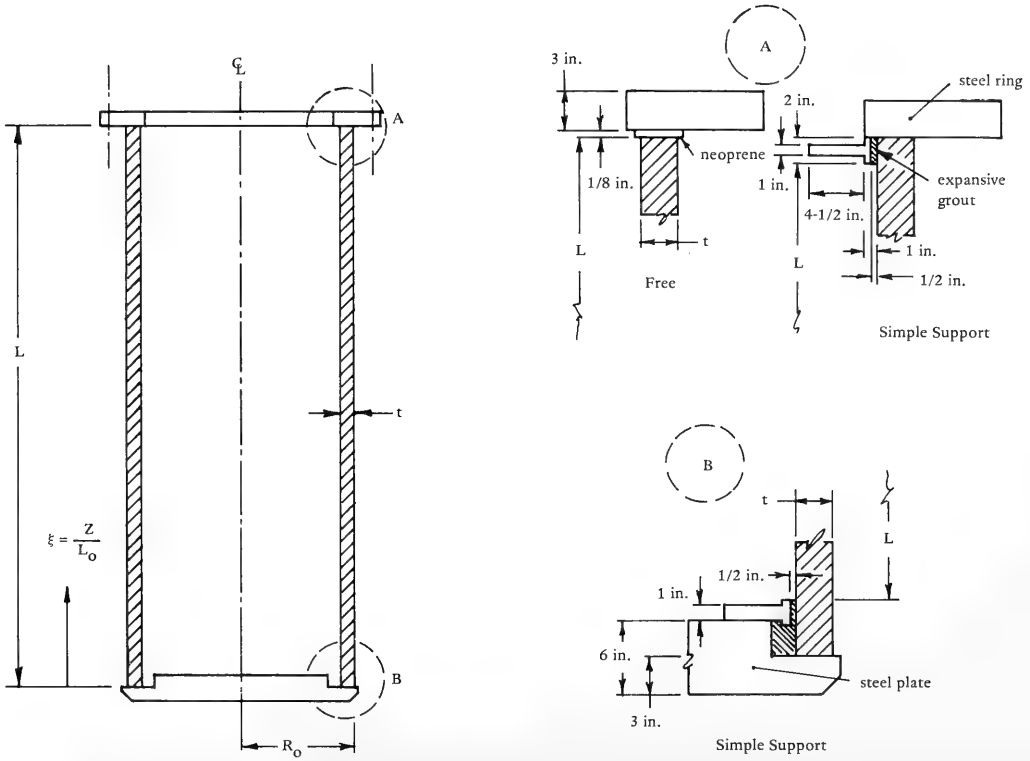

Figure B-4. Details of free- and simple-support end-conditions.

±0.002 in. (0.05 mm). The potentiometers were mounted on arms that extended from a center shaft. The center shaft was motor-driven at a rate of one revolution per 90 seconds.

Radial displacement calibration was accomplished by mounting aluminum shims of 0.125-inch (3.18-mm) thickness on the inside wall of the cylinder so that the steel ball passed over the shims to record magnitude and direction of inward displacement. These calibration marks also determined a 360-degree rotation.

The deflectometer system was insensitive to the axial orientation or lack of straightness of the center shaft. The top and bottom on the center shaft were fixed in location, and the shaft was rotated. The arms were fixed to the center shaft; and, in plan view, the end of each arm scribed a perfect circle. The steel ball at the end of each arm moved in and out to conform to the shape of the concrete cylinder. This radial movement was recorded as changes from a perfect circle.

In reducing the analog deflectometer data, an analog-to-digital converter was used along with a timing system to control the number of samples taken and the time interval between samples. Over 900 samples of analog data were digitized for each 360-degree rotation. This equates to a radial displacement data point every 0.17 inch (4.3 mm) around the inside circumference of the cylinder.

Strain Gages. Strain gaging of the specimens proved to be difficult because the concrete was in a wet condition. Various approaches for applying gages to wet concrete were tried, but none were successful. The problem was in maintaining the bond throughout the entire test.

The procedure for strain gaging is described as follows:

(1) Electrical-resistant strain gages (type FA-06-125, three-element rosettes) were mounted either on brass shim stock 0.002-inch (0.05 mm) thick or on steel shim

stock 0.005-inch (0.13-mm) thick and waterproofed, using standard procedures. These procedures used normal preparation steps for applying gages to metal and then were waterproofed using General Electric Clear RTV 109. This waterproofing approach works successfully under hydrostatic pressure loadings equivalent to thousands of feet of head. A second type of electrical resistant gage used was a self-encapsulated, waterproof, weldable gage.

(2) The objective was to apply these waterproof gages to the wet concrete surface with an adhesive of sufficient bonding strength that strain in the parent material is transferred through the epoxy adhesive, through the shim stock material, to the gage. To check the accuracy of these shim-stock mounted gages, a control test was conducted on an aluminum tube loaded in uniaxial compression. Seven pairs of gages were mounted on the aluminum cylinder; each gage in a pair was diametrically opposite the other gage. The test consisted of three pair of single wire gages mounted with Eastman 9-10, two pair of foil gages on brass shim stock mounted with EPY-150, one pair of foil gages on brass shim stock mounted with Eastman 9-10, and one pair of foil gages on brass shim stock mounted with Hysol EA 934. Eastman 9-10 is an excellent adhesive in a dry environment, so it was used in this test as a control. The results showed that gages mounted on brass shim stock registered accurate strains. The different glue systems did not affect the results.

(3) In the first method of mounting foil gages on brass shim stock to the wet-concrete specimens, an underwater curing adhesive developed at CEL (Ref 17) was

used. This method did not bond the shim stock to concrete for the duration of the test. A second method used epoxy adhesive Hysol EA 934, which was known to maintain a high bond strength when dry-concrete became wet (Ref 18). The strain data still indicated that the brass shim stock was not adhering to the concrete at the higher pressure (or strain) levels. The third method used Hysol adhesive again, but this time extra attention was paid to roughening the brass surface, deeply roughening the concrete surface (by grinding with silicon carbide grit) and, when applying the gage, embedding the edges of the brass shim stock in a thick bead of epoxy around the periphery. These additional steps also did not solve the problem. The fourth method was to try steel shim stock, instead of brass, and to use the procedures mentioned previously. At the same time, weldable gages were tried. None of these systems was successful; attempts at strain gaging were terminated. The deflectometer data were excellent, and additional potentiometers per test were used.

Television Camera. A closed-circuit television camera was installed at the top of each specimen. The video tape system recorded implosion. Although the frames per second rate did not permit detailed study of the failure zone, the circumferential location of failure could usually be defined and an interesting sequence of failure was recorded, including the sound of implosion.

High-Speed Camera. A high-speed motion picture camera was installed at the top of the specimens. It was hoped that a failure sequence could be filmed. The camera speed was initially set at 200 frames/sec which permitted 40 seconds of film time. The speed could

have been increased to 1,000 frames/sec, if desired. However, after several tests and no coverage of failure, the film speed was reduced to 100 frames/sec to increase the film time to 80 seconds. The camera was installed in eight specimens but failure coverage was not obtained in any test. The techniques used to try to predict imminence of failure are discussed in the Test Procedure section.

TEST PROCEDURE

The pressure vessel used in the tests had an inside diameter of 72 inches (1830 mm) and an operational pressure of 5,500 psi (37.9 MPa). The pressure load was created by pumping additional water into the vessel and thereby compressing the fluid. Freshwater was used in the tests.

The temperature of the water typically varied between 3° and 10°C for different tests; however, the temperature inside the specimens typically varied between 10° and 13°C. The higher temperature inside the specimens was due to warmer room temperature and lights for the television.

All specimens were placed in the pressure vessel on the evening before testing and allowed to soak in order that the degree of water saturation of the concrete for the different specimens would be the same. It was hoped that soaking overnight partially saturated the concrete to equal levels.

The rate of pressure application was 10 psi/min (0.069 MPa/min) between hold periods where data were recorded. Hold periods occurred at 25 psi (0.172 MPa) increments and typically lasted for 2.5 minutes. From the beginning to the end of the test, the overall pressurization rate was about 5 psi/min (0.034 MPa/min).

The television monitor was operated throughout the test. Its use was invaluable in operating the deflectometer system, detecting leaks, and recording implosion on videotape.

Several specimens leaked during the test. Most of the leaks occurred between the concrete and steel end-closures. However, some of the specimens had cracks through the wall and water slowly leaked through these cracks until the pressure load exceeded approximately 200 psi (1.4 MPa). Leaks did not affect the test results.

For the long-term loading tests, a digital comparator was used to control the operation of an auxiliary pressure pump and maintain the pressure load at ±2 psi (0.014 MPa).

Failure of the specimens was instantaneous, with literally a fraction of a second of advanced warning. High-speed motion picture film of failure was not obtained during eight attempts. In several of the cases, the film was exposed before implosion occurred. In the other cases, implosion occurred while the operator was waiting for an indication of failure. Methods used to indicate failure are described below.

(1) Radial Displacement - A real time signal from a potentiometer was displayed on an oscilloscope. During pressurization periods, the potentiometer was placed on the worst flat-spot (probable failure zone), and the rate of inward radial displacement with pressure was monitored. It was believed that an increase in the rate of change of radial displacements would indicate implosion. This was the case, but warning time was not sufficient to trigger a toggle switch to operate the camera.

(2) Acoustic Emissions - Acoustic emission transducers were placed on the pressure vessel head or on the top stiffener to record cracking activity of the concrete. It was hoped that the concrete would show considerably more cracking activity just before failure. This method was not successful because the acoustic emission activity of concrete is high and erratic in the

inelastic region. It was not possible to distinguish between spurts of activity and the activity just prior to failure.

(3) Pressure - The technician, who pressurized the specimen, closely watched pressure gages during the test. A pause in the rate of movement of a pressure gage needle would indicate imminent failure. For several of the tests there was no pause in needle movement; and for the tests with a pause, time was not sufficient to relay a message.

Upon removal, the specimens from the pressure vessel were inspected, photographed, and sketched. Fragments of concrete from failure zone sections were salvaged and pieced together for closer inspection of the failure zone.

It was at this stage that wall thickness measurements were made. The specimen was broken up, and the thickness of the pieces was measured with a micrometer. In this manner, numerous and accurate measurements of wall thicknesses were obtained.

SPECIMEN GEOMETRY

A summary of the specimen geometry is given in Table B-1. Data on maximum and minimum wall thicknesses are presented. Also, construction out-of-roundness data at the flat-spot locations are given. Typically, the minimum wall thickness coincided with the flat-spot location because this occurred at the outer mold seams. Table B-2 gives a digest of the out-of-roundness parameters. This presentation of data, however, is not truly descriptive of the out-of-round shape. Figure B-5 shows a cross-section at an elevation of 50 inches from the bottom, $\xi = 0.4$, of specimen 2-3. The initial out-of-round shape for the outer and inner mold are shown, using an exaggerated displacement

Table B-1. Specimen Geometry

Specimen No.	$\frac{t}{D_o}$	$\frac{L}{D_o}$	t^a (in.)	$t_{max}{}^b$ (in.)	$t_{min}{}^b$ (in.)	$\frac{\Delta t_{min}}{t}$	Construction Out-of-Roundness (Flat Spots) at or Near Failure Location					
							Inside Wall			Outside Wall		
							$\frac{\Delta R_i}{t}$	θ	ξ	$\frac{\Delta R_o}{t}$	θ	ξ
1-1	0.024	2.35	1.310	1.439	1.201	0.08	0.04	305	0.48	0.10	0	0.45
1-2	—	2.24	—	1.462	1.178	0.08	—	—	—	·	—	—
2-1	0.037	∞	1.975	2.047	1.874	0.05	0.03	175	0.50	0.05	180	0.45
2-2	—	(2.48)[c]	1.960	2.092	1.832	0.07	—	—	—	—	—	—
2-3	—	—	—	—	—	—	0.03	310	0.99	0.04	335	0.98
2-4	—	—	—	—	—	—	—	—	—		·	-
3-1	0.037	2.35	1.965	2.064	1.848	0.06	0.02	310	0.48	0.09	0	0.40
3-2	—	—	—	2.065	1.823	0.06	0.03	180	0.48	0.05	180	0.45
3-3	—	—	1.966	2.069	1.856	0.06	0.04	20	0.48	0.05	180	0.45
3-4	—	—	—	·	—	—	—	—	—	—	—	—
4-1	0.037	2.35	—	—	—	—	0.04	170	0.48	0.07	180	0.37
4-2	—	—	—	—	—	—	0.03	170	0.48	0.04	175	0.70
4-3	—	—	—	—	—	—	0.02	25	0.48	0.07	0	0.45
5-1	0.063	∞	3.392	3.588	3.255	0.04	0.02	180	0.50	0.03	145	0.98
5-2	—	(2.48)[c]	—	—	—	—	—	—	—	—	·	—

[a] Between 100 and 250 readings.

[b] Average value from 6-in.-sq fragmented area of imploded specimen.

[c] Actual specimen L/D_o.

Table B-2. Digest of Specimen Out-of-Roundness

$\frac{t}{D_o}$	Out-of-Roundness Parameters		
	$\frac{\Delta t_{min}}{t}$	$\frac{\Delta R_i}{t^a}$	$\frac{\Delta R_o}{t^a}$
0.024	0.08	0.04	0.10
0.037	0.06	0.03	0.06
0.063	0.04	0.02	0.03

[a] Radius deviations are for radii less than the nominal radii.

scale. In the regions of 0 and 180 degress, it is observed that the wall is thinner than nominal and that the curvature is flatter than that of the membrane circle. The center of the membrane circle for the outer wall is offset from the center of the inner wall by about 0.02 inches.

Another cross-sectional view at elevation $\xi = 0.4$ is shown in Figure B-6. The data are a compilation from several specimens of $t/D_o = 0.037$.

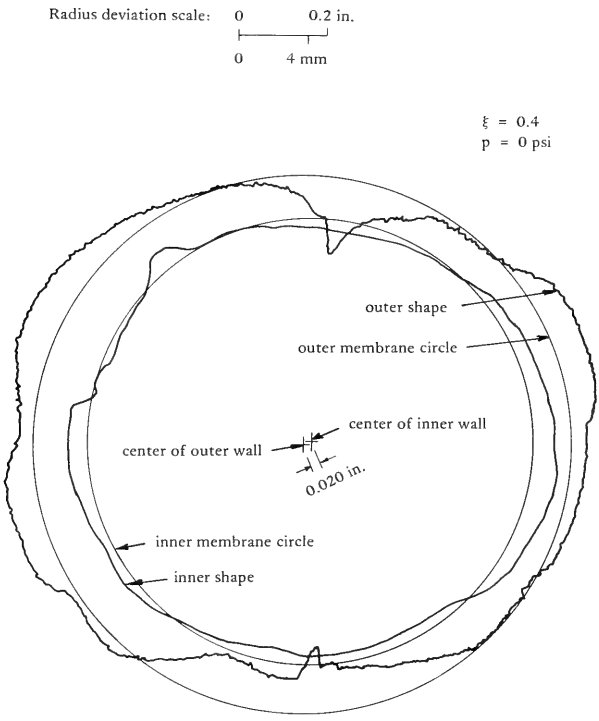

Figure B-5. Initial cross-section shape (superimposed to show relative changes in wall thickness and flat spots) for specimen 2-3, showing radius deviations of inner and outer wall surfaces at 0 psi and $\xi = 0.4$ (50 inches from bottom).

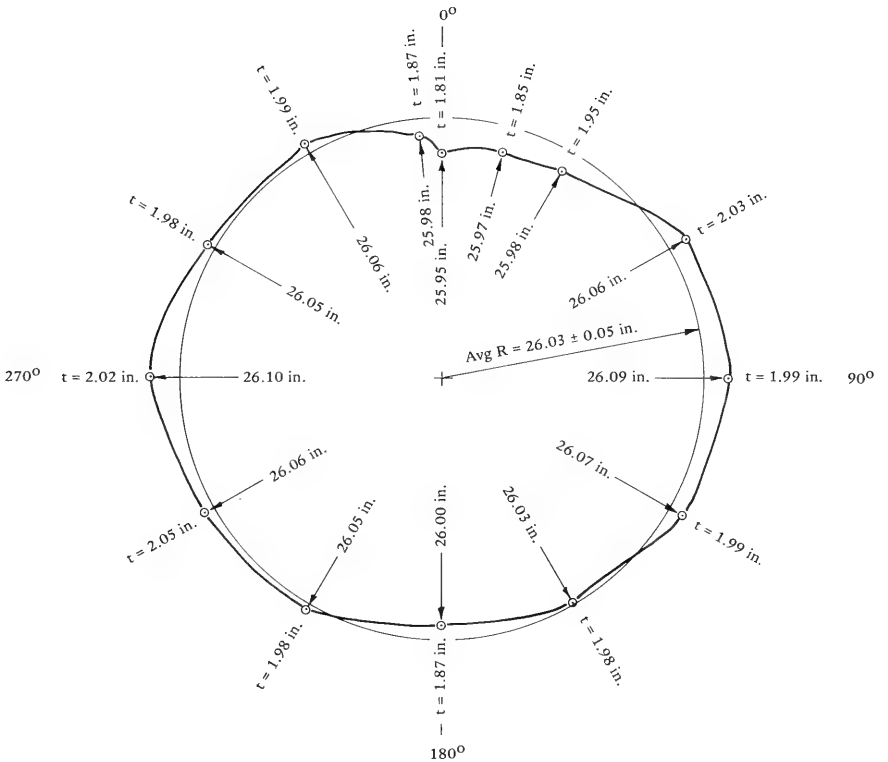

Figure B-6. Variation in wall thickness and mean radius at different locations on circumference at $\xi = 0.4$ (50 inches from bottom). Values are average of several specimens.

Variations in wall thickness and mean radius, R, are shown around the circumference. The average R was 26.03 ± 0.05 inches (661 ± 1 mm). The magnitude of the standard deviation was mostly from the lack of accuracy in measuring the radius with the steel rule.

CONCRETE MATERIALS

Mix Design

Concrete was batched and supplied by a transit mix company. Each delivery consisted of 2.0 yd^3 (1.5 m^3) of concrete. The mix was designed for 6,000 psi (41 MPa) at 28 days. The proportions of cement to sand to aggregate were 1:1.96:2.22, respectively. The cement content was 676 lb/yd^3 (401 kg/m^3). Water-to-cement ratio averaged 0.55. Slump at the time of placement controlled the total water content, and the slumps averaged 3-3/4 ± 1/4 inches (95 ± 6 mm).

Portland, low alkali, type II cement was used along with a water-reducing admixture, Zeecon H, at a rate of 6 ounces (0.17 kg) per 100 pounds (45.4 kg) of cement. The sand and aggregate were from the Santa Clara River Basin. Maximum aggregate size was 3/8 inch (9.5 mm), and the aggregate underwent heavy media separation.

A summary of the concrete properties is given in Table B-3. The concrete compressive strengths were measured at 7 and 28 days and at the time of testing. Stress-strain curves were obtained from numerous specimens. Several modulus parameters are listed in Table B-3, along with the ultimate strain and Poisson's ratio. Figure B-7 shows representative stress-strain curves for 7,000 and 8,000 psi (48 and 55 MPa) concrete.

Expansive-cement grout, used as a packing material between the stiffeners and concrete wall, had mix proportions of one part portland cement type K, one part San Gabriel River sand between sieve sizes 4 and 16, one part San Gabriel River sand between sieve sizes 16 and 30.

Table B-3. Material Properties of Concrete

Specimen No.	Compressive Strength, f'_c, at Age –		Material Properties at Age of Test							
	7 Days[a] (psi)	28 Days[a] (psi)	Compressive[b] Strength at Age of Test, f'_c (psi)	Coefficient of Variation (%)	Age (days)	Initial Modulus, $E_i \times 10^6$ (psi)	Secant Modulus to 0.5 f'_c, $E_S \times 10^6$ (psi)	Tangent Modulus at 1.0 f'_c, $E_T \times 10^6$ (psi)	Ultimate Strain, $\epsilon_u \times 10^{-3}$ (in./in.)	Poisson's Ratio, ν
1-1	2,740	6,760	7,650	2.5	85	3.9	3.9	1.2	2.8	0.17
1-2	2,880	6,400	8,310	1.8	84	–	–		–	–
2-1	4,200	6,200	6,780	6.3	78	3.9	3.7	1.5	2.4	0.15
2-2	5,660[c]	6,630	8,690	4.8	186	5.0	4.6	1.7	3.1	0.17
2-3	–	6,330	6,740	5.3	50	–	–			–
2-4	4,730	6,230	7,820	3.1	113	4.3	4.0	2.0	2.3	0.19
3-1	5,000	6,330	7,190	3.5	89	3.8	3.7	1.7	2.5	–
3-2	5,370	6,330	6,830	9.2	105	3.5	3.5	1.5	2.6	
3-3	–	6,170	6,870	2.8	56			–	–	
3-4	4,500	6,130	8,170	7.1	157	4.0	4.0	1.7	2.5	0.25
4-1	5,200	6,400	9,340	2.3	218	–		–		
4-2	4,430	6,330	7,310	9.8	133	4.2	4.0	1.5	2.2	0.16
4-3	4,400	5,700	8,020	9.2	217	4.8	4.3	1.8	2.7	0.21
5-1			7,990	2.2	295	4.3	4.3	1.4	2.4	0.17
5-2			8,570	2.7	335	–		–		–

[a] Average of three specimens, 6x12-in. size.

[b] Typical average of six specimens, 6x12-in. size.

[c] Age 14 days.

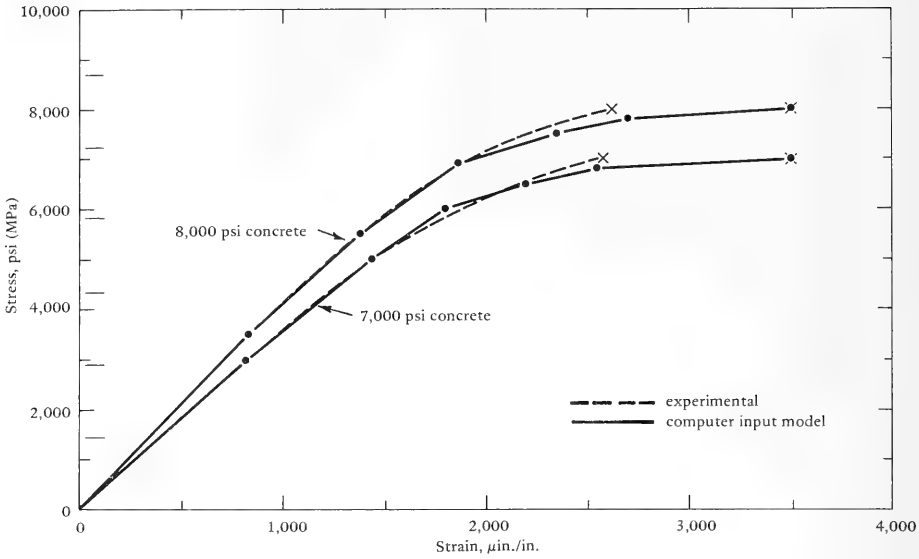

Figure B-7. Uniaxial compressive stress-strain relationship for concrete.

The water-to-cement ratio was 0.37 and a retardant admixture, E42 Master Builder, was used at 4.1 ounces (0.12 kg) per 100 pounds (45.4 kg) of cement. The compressive strength of this mix was 5,520 psi (38.1 MPa) at 7 days taken from three 3x6-inch (76x152-mm) control cylinders.

TEST RESULTS

Implosion

Test conditions and implosion results are presented in Table B-4. The implosion pressure, P_{im}, and nondimensional ratio of implosion strength, P_{im}/f'_c, are given along with data on the failure hole size and boundary behavior.

A summary of the implosion results is given in Table B-5.

Table B-4. Test Conditions and Results

Specimen No.	Test Conditions				Test Results								Remarks
	Preload Pressure (psi)	Pressure Rate (psi/min)	Boundary Condition	Type of Loading	Implosion Pressure, P_{im} (psi)	$\frac{P_{im}}{f'_c}$	Failure Zone				Boundary Behavior		
							θ_1	θ_2	θ_3	ξ	ϕ	ξ	
1-1	25	4.2	simple	short	300	0.039	320	50	0	0.40	0.40	0.08	–
1-2	25	3.0	simple	short	329	0.040	320	60	0	0.45	–	–	–
2-1	75	4.0	free	short	406	0.060	140	230	180	0.54	0.90	0.04	–
2-2	75	5.1	free	short	400	0.046	285	15	330	0.94	–	–	–
2-3	75	4.9	free	short	368	0.055	285	15	330	0.94	0.60	0.04	–
2-4	75	5.2	free	short	330	0.042	260	330	300	0.07	0.96	0.01	Casting defect in failure zone.
3-1	75	5.0	simple	short	550	0.076	140	240	180	0.37	0.35	0.03	
3-2	75	4.6	simple	short	575	0.084	140	230	180	0.40	0.23	0.02	–
3-3	75	5.3	simple	short	525	0.076	300	60	0	0.45	0.15	0.02	–
3-4	75	6.4	simple	short	342	0.042	30	105	75	0.18	0.68	0.08	Severe casting defect.
4-1	75	5.5	simple	long	620	0.066	135	210	180	0.36	0.51	0.08	2.5 hrs at 620 psi.
4-2	75	5.7	simple	long	590	0.081	120	220	180	0.69	0.15	0.02	Accidental failure 44 hrs at 475 psi.
4-3	75	5.5	simple	long	615	0.077	315	70	20	0.54	0.08	0.02	168 hrs at 450 psi.
5-1	100	5.2	free	short	1,078	0.135	100	230	180	0.91	–	-	Uneven bearing support, failure mode like Group 2.
5-2	150	10.4	free	short	880	0.103	95	115	105	0.98	–	–	Uneven bearing support, very local failure.

Table B-5. Summary of Test Results

Group	t (in.)	$\frac{t}{D_o}$	$\frac{L}{D_o}$	Boundary Condition	Type of Loading	f'_c (psi)	P_{im} (psi)	$\frac{P_{im}}{f'_c}$	Coefficient of Variation (%)	Remarks
1	1.31	0.024	2.30	simple	short	7,980	315	0.039	0.7	–
2	1.97	0.037	∞	free	short	7,400	391	0.053	13.1	Specimen 2-4 excluded
3	1.97	0.037	2.35	simple	short	6,960	550	0.079	5.6	Specimen 3-4 excluded
4	1.97	0.037	2.35	simple	long	8,220	608	0.075	9.9	–
5	3.39	0.063	∞	free	short	7,990	1,078	0.135	–	Specimen 5-2 excluded

Post-implosion views of several specimens are shown in Figures B-8 through B-16. For those specimens having a simple-support boundary condition, the failure holes occurred in the midlength region away from the ends (Figures B-8 and B-13). For those specimens having a free-support boundary condition, the failure hole typically occurred at the top end (Figures B-11 through B-15), but the failure hole occurred in the midlength region for specimen 2-1 (the strongest Group 2 specimen) (see Figure B-10).

The experimental test setup was probably the cause for the failure holes that occurred at the top. When the specimens were fabricated, the top cylinder edge was hand-troweled and therefore uneven. On specimen 5-1 the top end-closure ring was placed on the cylinder without the gasket material to observe unevenness. A rather large portion of the mating surface showed a gap of from 1/16 to 1/8 inch (2 to 3 mm). A filler material, such as gypsum used in specimens 2-1 and 5-1, filled the gap adequately. However, use of the gypsum was discontinued because the material is water soluble, so small leaks grew into major leaks. Epoxy was used as its replacement, but epoxy filler material did not appear to perform adequately. Epoxy has a modulus about one-tenth that of concrete and probably about one-fifth that of gypsum. It wasn't until after specimen 5-2 was tested (at the end of the test program) that it became quite apparent that the epoxy filler

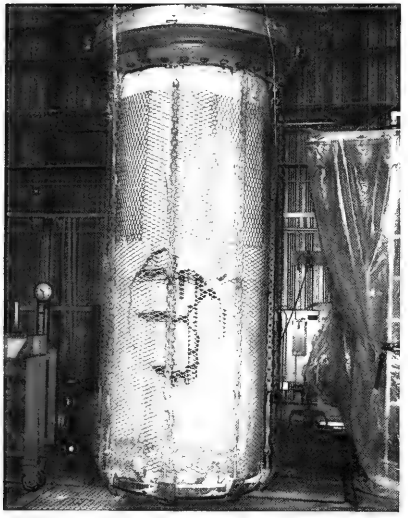

Figure B-8. Post-implosion view of specimen 1-1 (t/D_o = 0.024, simple support).

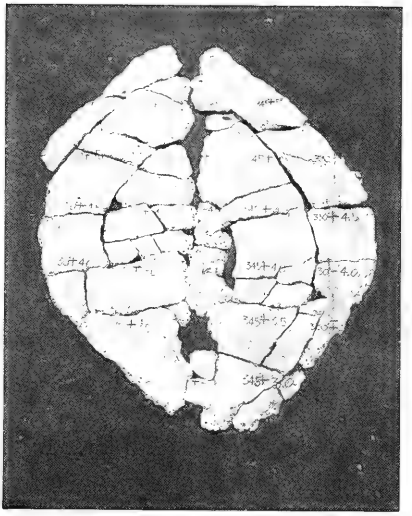

Figure B-9. Fragments of failure hole from specimen 1-1.

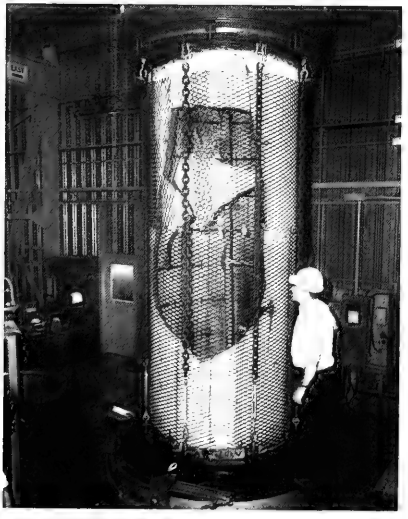

Figure B-10. Post-implosion view of specimen 2-1 (t/D_o = 0.037, free support).

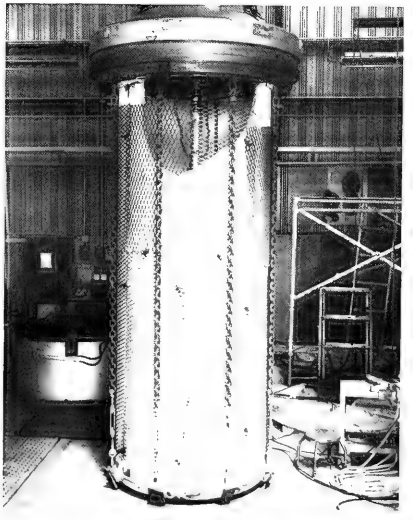

Figure B-11. Post-implosion view of specimen 2-2 (t/D_o = 0.037, free support).

material was not a good substitution. Figure B-16 shows that specimen 5-2 had a very local failure at the top edge which was a bearing-type failure.

Boundary behavior is quantified in Table B-4. For convenience, a nondimensional value, ϕ, was selected to express boundary behavior as the ratio of radial displacement at the end supports to the radial displacement at midlength of the specimen. A rigid support would be identified by $\phi = 0$ and a free support by $\phi = 1$.

Observed boundary performances showed a small difference between actual and theoretical behavior. For free-support specimens the ideal ϕ of 1.00 was closely approximated. Two specimens with $t/D_o = 0.037$ showed free-support behavior where ϕ was 0.90 and 0.96. Specimen 2-3 showed unusual behavior where the bottom of the cylinder moved radially inward the least, $\phi = 0.60$, but the top moved inward the most, $\phi = 1.36$ (i.e., the top of the cylinder at the flat spot location moved inward more than the middle).

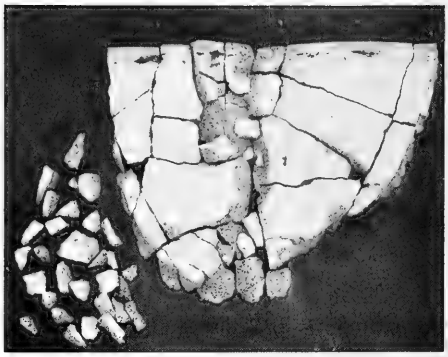

Figure B-12. Fragments of failure hole from specimen 2-2.

Figure B-13. Post-implosion view of specimen 3-1 ($t/D_o = 0.037$, simple support).

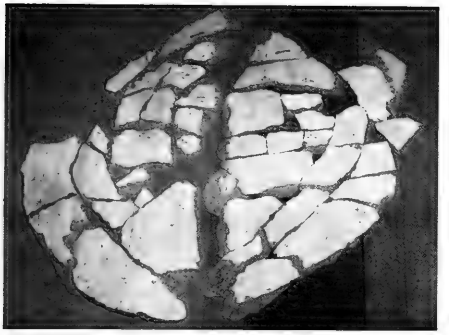

Figure B-14. Fragments of failure hole from specimen 3-1.

For simple-support specimens, the ideal ϕ of zero was not obtained. The radial deflection of the steel stiffener provided some compliance. The stiffener deflection was calculated to be about 0.01 inch (0.3 mm) at a pressure load of 500 psi (3.5 MPa), or a ϕ of 0.08. Measured radial deflections showed values about 0.02 inch (0.5 mm), a

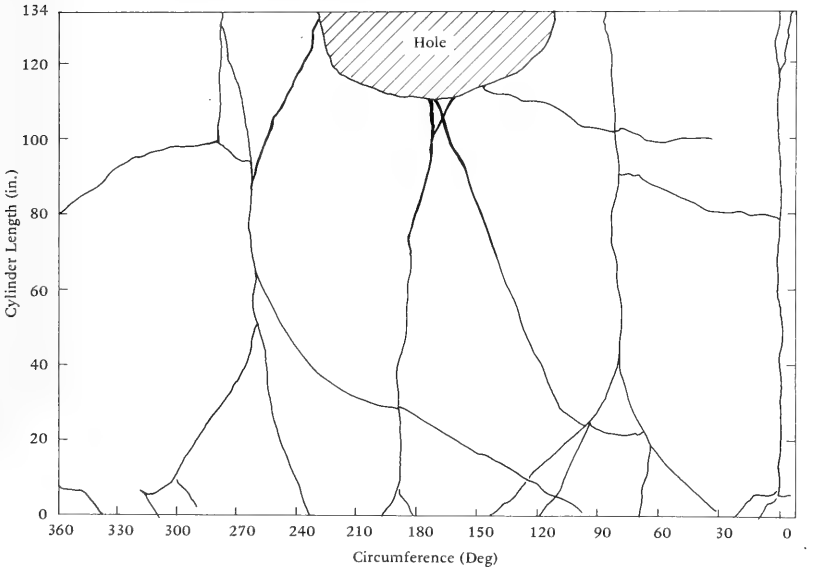

Figure B-15. Post-implosion view of specimen 5-1 (t/D_o = 0.063, free support).

ϕ of about 0.16, at a distance of 2 inches (50 mm) away from the stiffeners. The test specimens had a clear length between stiffeners of 127 inches (3220 mm). After accounting for the compliance of the stiffener, the "actual" length of the cylinder appeared to be about 130 inches (3300 mm); hence, the effect of stiffener compliance was small.

Figure B-16. Local failure of specimen 5-2 (t/D_o = 0.063, free support).

To test for possible reduction in implosion strength due to sustained loading, the implosion resistance of Group 4 specimens was assumed to be equal to that of the average value of Group 3 specimens; i.e., P_{im}/f'_c = 0.079. Specimen 4-1 was subjected to 85% of this load. After 2.5 hours of load exposure the specimen imploded, which implied a strength reduction of 15% for a relatively brief period of sustained

loading. Subsequently, the sustained pressure for specimen 4-2 was lowered to 80% of predicted short-term strength, while specimen 4-3 was subjected to 70%.

Specimen 4-2 was accidently imploded after 44 hours of load exposure during modification of the electronic pump control equipment; no record of the actual implosion pressure was obtained. The implosion value listed in Table B-4 was based on a calculated estimate of the pressure increase in the vessel for a known duration of pump operation. Data were available on the exact time of operation of the pump before implosion occurred. The estimated implosion pressure is probably within a 5% error limit.

Specimen 4-3 withstood a pressure load of 450 psi (3.1 MPa) for 168 hours without incident. The pressure was then reduced to zero where it remained for 16 hours before the specimen was subjected to 85% of short-term strength. The pressure level was sustained for 2.5 hours without any signs of major structural distress, then the pressure level was raised to 95% where implosion occurred after 3 minutes.

Radial Displacement Behavior

Radial displacement terms are defined diagrammatically in Figure B-17. The deflectometer instrumentation method measured radial displacement from initial to deflected shape, w. Membrane radial displacements, w_m, were determined from the w data. The following method was used. The reader should picture radial displacement data being displayed on oscillograph paper as a potentiometer moves around the circumference of a cylinder. A straight line would mean a perfect circle. The specimens were not perfect; therefore, the line moved upward (for inward displacement) and downward (for outward displacement). The wavy line on the oscillograph paper is a chart of out-of-roundness data. The wavy line can be digitized (i.e., each point along the line can be given a magnitude value). The average of these values is plotted as a straight line and represents the membrane curve. The average defines the size or radius of the membrane circle.

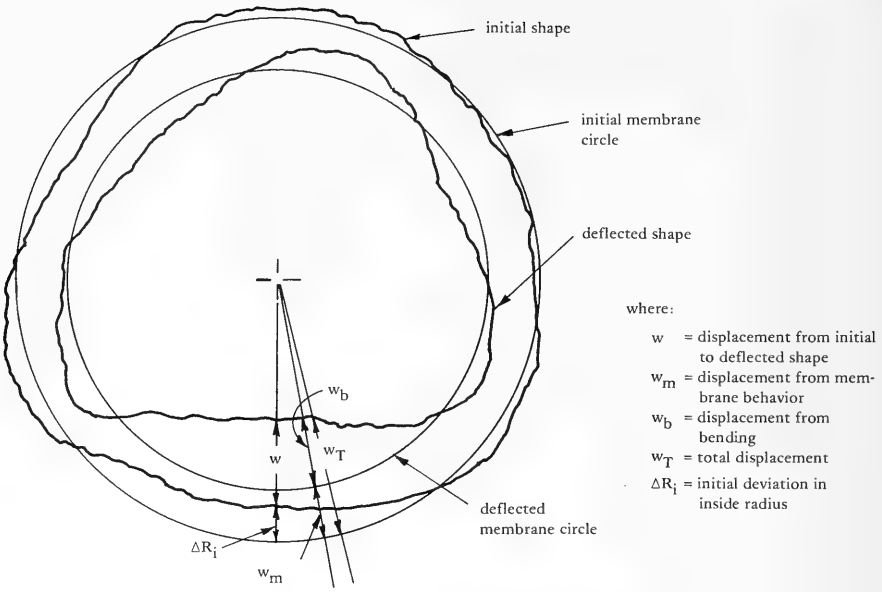

Figure B-17. Definition of displacement terms.

When a deflected shape was plotted the reference point was the location of the center shaft that held the potentiometer; however, this location was not the "true" center of the deflected shape. The operation of finding the true center location was that of manually superimposing the membrane curve on the deflected shape and using judgment to decide the location. Judgment was based on fitting the membrane curve (perfect circle) of known size to the deflected shape such that the area between the wavy line and the membrane curve was divided equally.

The initial and deflected cross-sectional shapes of a free and simply supported specimen with their corresponding membrane circles are shown in Figures B-18 and B-19, respectively. All specimens having a free support deflected into an elliptical shape where the number of lobes, n, was 2. All specimens having a simple support deflected into a shape with n = 3.

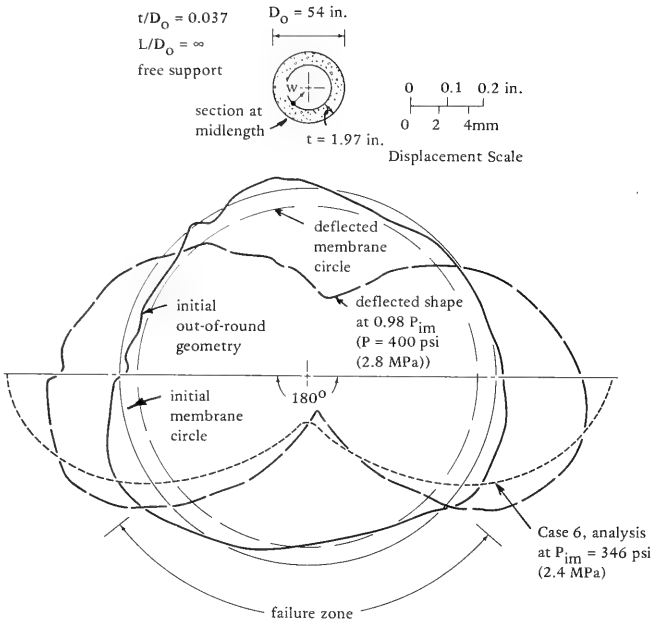

Figure B-18. Initial and deflected cross section at midlength of typical cylinder having t/D$_o$ = 0.037 and free support.

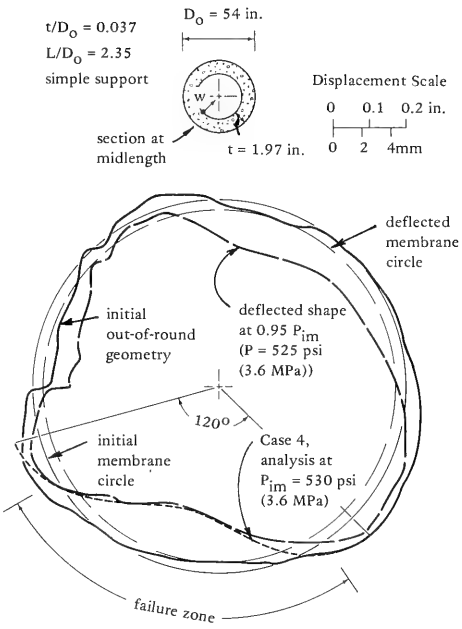

Figure B-19. Initial and deflected cross section at midlength of typical cylinder having t/D$_o$ = 0.037 and simple support.

The worst flat spot on each cylinder eventually became the failure location; this location consistently coincided with the wall sections that were thin and somewhat flat initially.

Radial displacement data, as shown in Figures B-18 and B-19, were plotted at various pressure levels for the test specimens. Data obtained from these plots were used in analyzing the structural behavior.

Pressure versus w and w_m relationships are shown in Figures B-20 through B-22.* The data for w are from the worst flat spot location. The w_m curves come from w data so the maximum pressure for the w_m curve (experimental perfect cylinder) cannot exceed P_{im} of the experimental out-of-round specimen.

Radial displacement behavior along the length of the cylinder is shown in Figures B-23 through B-25. The influence of the boundary condition as it is affected by the simple-support and the free-support conditions is vividly seen.

Radial displacement data for specimens 5-1 and 5-2 were recorded, but meaningful data were not obtained because the end-closures shifted position as the pressure load was increased. The center of the shaft moved, which meant that a common reference point between various pressure levels was not available.

In Figure B-17, it is observed that the total radial displacement, w_T, is equal to:

$$w_T = w + \Delta R_i \tag{B-1}$$

and

$$w_T = w_m + w_b \tag{B-2}$$

---

*The analytical curves will be discussed later.

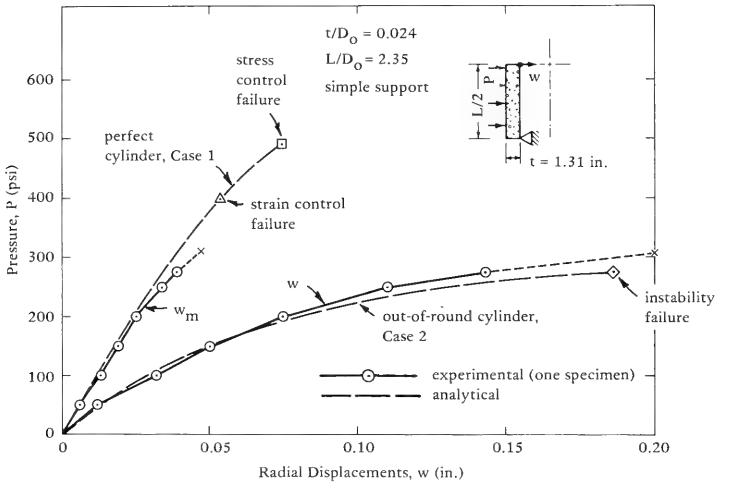

Figure B-20. Radial displacement behavior at midlength of specimen 1-1 having t/D_o = 0.024 and simple support.

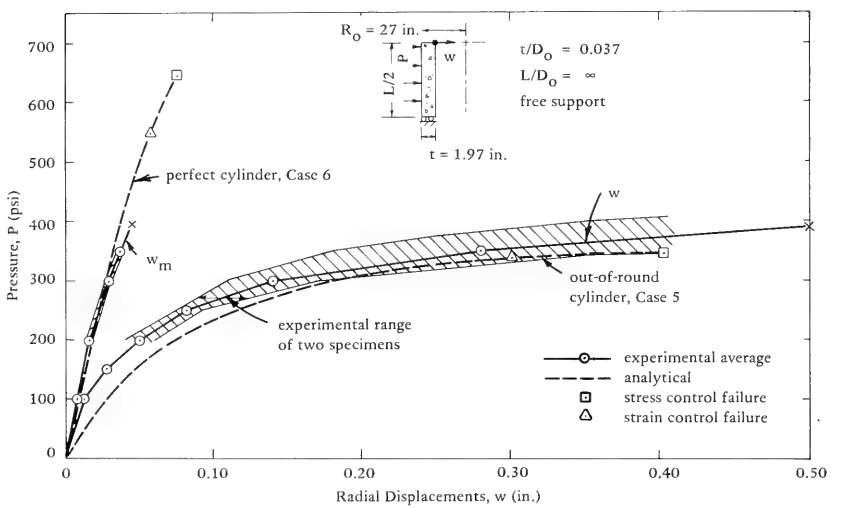

Figure B-21. Radial displacement behavior at midlength of Group 2 cylinders having t/D_o = 0.037 and free support.

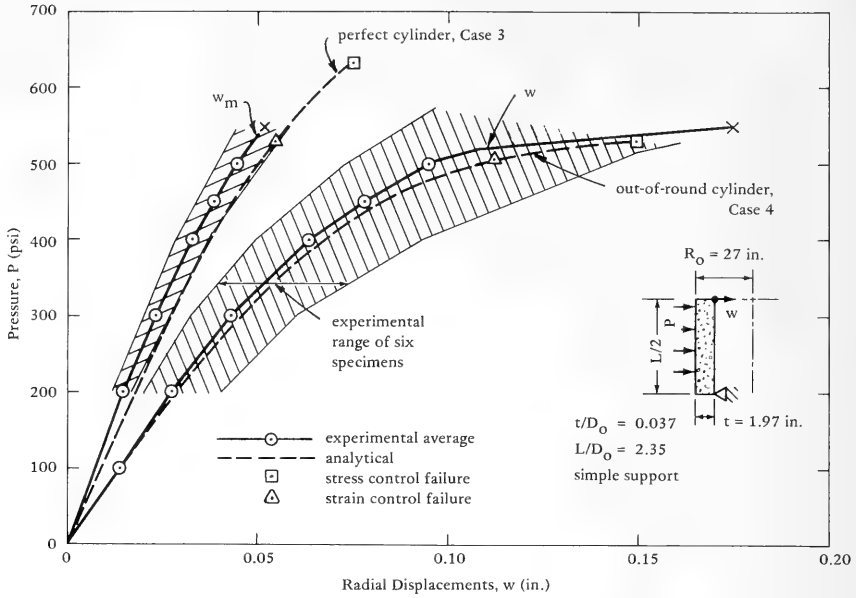

Figure B-22. Radial displacement behavior at midlength of Group 3 cylinders having $t/D_o = 0.037$ and simple support.

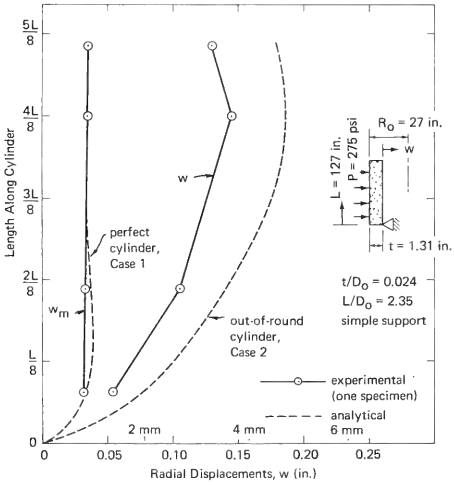

Figure B-23. Radial displacement behavior along length of specimen 1-1 having $t/D_o = 0.024$ and simple support at a pressure load of 0.89 P_{im}.

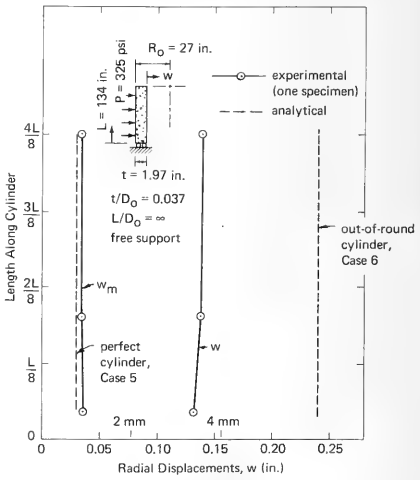

Figure B-24. Radial displacement behavior along length of specimen 2-1 having $t/D_o = 0.037$ and free support at a pressure load of 0.78 P_{im}.

The known terms are w, w_m, and ΔR_i. Hence, radial displacements due to bending can be calculated as:

$$w_b = w + \Delta R_i - w_m \qquad \text{(B-3)}$$

An estimate of the magnitude of strain on the inside and outside wall surfaces can be made because w_m and w_b are now known. Membrane strain is calculated from:

$$\varepsilon_m = \frac{w_m}{R_i} \qquad \text{(B-4)}$$

and bending strain is calculated from an expression developed in Reference 19 as:

$$\varepsilon_b = \frac{w_b\, t}{2\, R^2}(n^2 - 1) \qquad \text{(B-5)}$$

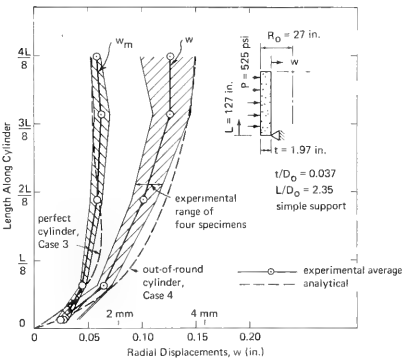

Figure B-25. Radial displacement behavior along length of Group 3 cylinders having $t/D_o = 0.037$ and simple support at a pressure load of $0.95P_{im}$.

Table B-6 summarizes the ultimate radial displacements and calculated strains. It is interesting to note that although w_b is typically several times the magnitude of w_m, the calculated strains ε_m and ε_b are nearly equal. At implosion the strains at the flat-spot location on the inside wall experienced slight tension while on the outside wall strains were on the order of 4,000 μin./in. compression.

Table B-6. Ultimate Radial Displacements and Calculated Strains

Group	No. of Specimen	n	ΔR_j (in.)	w (in.)	w_m (in.)	w_b (in.)	ϵ_m (μin./in.)	ϵ_b (μin./in.)	Strains at Flat Spot on –	
									Inside Wall, $\epsilon_m - \epsilon_b$ (μin./in.)	Outside Wall, $\epsilon_m + \epsilon_b$ (μin./in.)
1	1	3	0.050	0.200	0.043	0.207	1,670	1,560	+110	+3,230
2	2	2	0.057	0.508	0.051	0.514	2,040	2,240	–200	+4,280
3	4	3	0.042	0.185	0.052	0.175	2,080	2,040	–40	+4,120
Average									–110 tension	+3,880 compression

ANALYTICAL RESULTS AND DISCUSSION

Analysis Description

A structural analysis was performed on the experimental specimens using a finite element method called NONSAP-A that incorporated an advanced constitutive relation subroutine for the concrete. The analysis was conducted by Chen, Chang, and Suzuki (Ref 20) without the benefit of the test results. Information on specimen geometry (including the out-of-round geometry, boundary conditions, and material properties) was supplied. It was desired to computationally model the test specimens as realistically as possible and then determine the accuracy of the predictions.

Constitutive Model. The constitutive model was developed in three parts - elastic, plastic and fracture - for concrete under general stress states.

For elastic concrete, it was assumed that, initially, concrete is an isotropic homogeneous linear elastic material and its stress-strain relations are described completely by two elastic constants, Poisson's ratio, ν, and Young's modulus, E. For the present analysis, $\nu = 0.19$ was used, and $E = 3.66 \times 10^6$ and 4.19×10^6 psi (25.2 and 28.9 GPa) were

determined from Figure B-7. The elastic limit envelope in general stress space was obtained by scaling the fracture envelope down to a size where uniaxial yield point corresponded to about 43% of the uniaxial strength.

For plastic concrete, a strain-hardening plasticity model as proposed previously in Reference 21 was used to describe the nonlinear irreversible stress-strain response of concrete material. The plastic incremental stress-strain relationship based on the normality flow rule in the theory of plasticity are developed in detail in Reference 22.

For fracture, the concrete failed when the state of stress reached a certain critical value. Two different types of fracture mode are defined here.

(1) "Cracking" Type - When the principal stresses are either in the tension-tension state or tension-compression state and their values exceed the limit values.

(2) "Crushing" Type - When the principal stresses are in the compression-compression state and their values exceed the limit values. When concrete cracks, the material is assumed to lose only its tensile strength normal to the crack direction but to retain its strength parallel to the crack direction. On the other hand, when concrete crushes, the material element loses its strength completely.

In the present analysis, a dual representation of fracture criterion was expressed in terms of both stresses and strain and specifies the limit value under multiaxial state of stresses or strains in the following forms:

(1) Stress Criterion

$$f(\sigma_{ij}) = J_2 + \frac{1}{3} A_u I_1 + \alpha I_1^2 = \tau_u^2 \quad \text{(B-6)}$$

where A_u and τ_u are material constants and where α is equal to zero when the principal stresses are in the compression state and equal to -1/6 when in the tension-compression or tension-tension state. The first invariant, I_1, corresponds to the mean stress component of the stress state. The term J_2 is the second invariant of deviatoric stresses.

(2) Strain Criterion

$$g(\varepsilon_{ij}) = J_2' + \frac{A_u}{3}\left(\frac{\varepsilon_u}{f_c'}\right) I_1' = \tau_u^2 \left(\frac{\varepsilon_u}{f_c'}\right)^2 \quad \text{(B-7)}$$

or

$$\text{Maximum of the Principal Strains} = \varepsilon_t \quad \text{(B-8)}$$

in which I_1' corresponds to volumetric strain and J_2' is the second invariant of deviatoric strains. The terms ε_u and ε_t specify the maximum ductilities of concrete under uniaxial compressive and tensile loading conditions, respectively. Herein, the compressive cylinder strength was assumed as 7,000 and 8,000 psi (48 and 55 MPa); and maximum compressive strain, ε_u, was 3,500 μin./in. The tensile strength, f_t', was assumed to be 0.09 f_c'; and maximum tensile strain, ε_t, was 800 μin./in. When the stress state in the concrete satisfied either the stress criterion (Equation B-6) or the strain criteria (Equations B-7

and B-8), fracture of concrete was assumed to occur. If the fracture stress state lies in the tension-compression or tension-tension zone, a crack was assumed to occur in a plane normal to the direction of the offending principal tensile stress or strain.

Finite Element Program. In the present work all the analyses were performed using NFAP program (Ref 23) on computer system IBM model 370-158. NFAP is a modified and extended version of NONSAP-A program (Ref 24), which is a modified version of the NONSAP program originally developed by Bathe, Wilson, and Iding (Ref 25). The present concrete constitutive model has been incorporated as a subroutine in the NFAP program. The average computing time for the two-dimensional (plane strain or axisymmetric) problems was about 5 minutes for each case. The average computing time for each three-dimensional analysis was about 62 minutes.

Geometry of Analysis. The eight cases as listed in Table B-7 were analyzed using isoparametric shell elements.

(1) Cases 1 and 3 were modeled as axisymmetrical problems with simple-support end-condition.

(2) Cases 5 and 7 were modeled as plane strain, axisymmetrical problems.

(3) Cases 6 and 8 were modeled as plane strain, asymmetrical problems. Out-of-roundness in the form of n = 2 (see Table 2) was included in the analysis.

(4) Cases 2 and 4 were treated as three-dimensional problems with large displacement. Out-of-roundness in the form of n = 3 was included in the analysis.

Table B-7. Analytical Results

Case No.	$\frac{t}{D_o}$	End Support	Circularity	Geometry of Analysis	f_c' (psi)	$(P_{im})_\epsilon$[a] (psi)	$(P_{im})_\sigma$ (psi)	$\frac{(P_{im})_\epsilon}{f_c'}$	$\frac{(P_{im})_\sigma}{f_c'}$	Mode of Failure	$\frac{(P_{im})_\epsilon / f_c'}{P_{im}/f_c'}$[b]	$\frac{(P_{im})_\sigma / f_c'}{P_{im}/f_c'}$[b]
1	0.024	simple	perfect	axisymmetric	8,000	398	478	0.050	0.060	material	–	–
2	0.024	simple	OOR[c]	3-D, n = 3	8,000	275	275	0.034	0.034	instability	0.85	0.85
3	0.037	simple	perfect	axisymmetric	7,000	531	632	0.076	0.090	material	–	–
4	0.037	simple	OOR	3-D, n = 3	7,000	508	530	0.073	0.076	material	0.92	0.96
5	0.037	free	perfect	plane strain	7,000	548	644	0.078	0.092	material	–	–
6	0.037	free	OOR	plane strain, n = 2	7,000	341	346	0.049	0.049	material	0.91	0.91
7	0.063	free	perfect	plane strain	8,000	1,056	1,320	0.132	0.165	material	–	–
8	0.063	free	OOR	plane strain, n = 2	8,000	960	1,088	0.120	0.135	material	0.89	1.00

[a] Failure defined by 0.08% tensile radial strain in all cases, not by excessive compressive strain.

[b] P_{im}/f_c' from Table B-5.

[c] OOR = out-of-round.

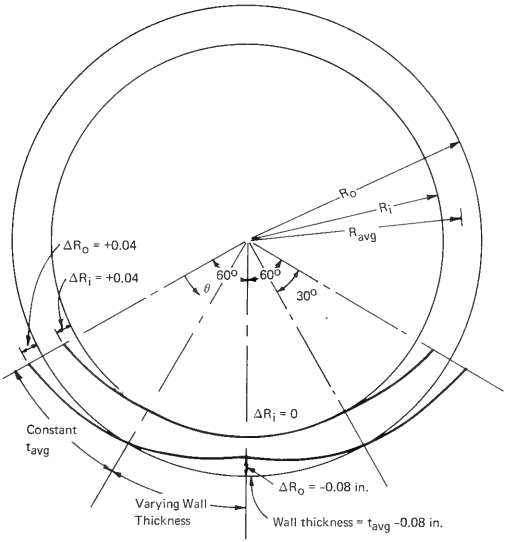

Figure B-26. Idealized initial out-of-round shape for cylinders with n = 3.

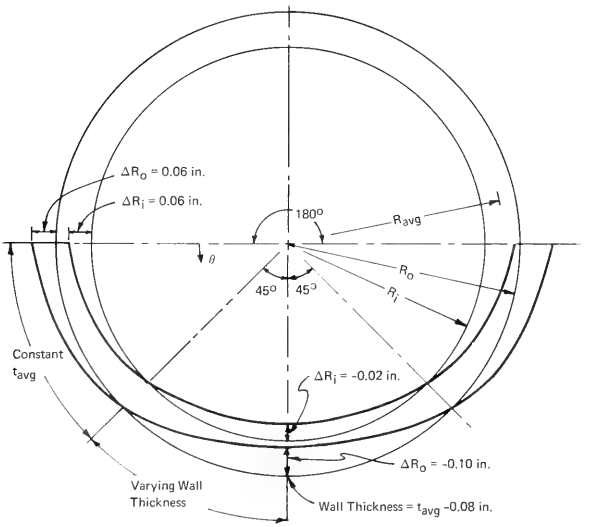

Figure B-27. Idealized initial out-of-round shape for cylinders with n = 2.

Cross-sectional geometry for the cylinders, which includes data on idealized out-of-roundness, is shown in Figures B-26 and B-27 with geometry values given in Table B-8.

Table B-8. Cross-Sectional Geometry for Cylinders

Case No.	$R_{avg_{0^o}}$ (in.)	ΔR (in.)	t_{0^o} (in.)	t_{60^o} (in.)	t_{90^o} (in.)	Numbers of Lobes, n[a]
1	26.345	0	1.31	–		0
2	26.345	0.04	1.31	1.23	–	3[b]
3	26.015	0	1.97	–	–	0
4	26.015	0.04	1.97	1.89	–	3[b]
5	26.015	0	1.97	–	–	0
6	26.015	0.06	1.97	–	1.89	2[c]
7	25.305	0	3.39	–		0
8	25.305	0.06	3.39	–	3.31	2[c]

[a] $\underline{n = 2}$ $\quad R_{avg} = R_{avg_{0^o}} + \Delta R \cos 2\theta$

$$t \begin{cases} t_{0^o} & 0^o \leq \theta \leq 45^o \\ t_{0^o} + \dfrac{t_{90^o} - t_{0^o}}{45^o}(\theta - 45^o) & 45^o \leq \theta \leq 90^o \end{cases}$$

$\underline{n = 3}$ $\quad R_{avg} = R_{avg_{0^o}} + \Delta R \cos 3\theta$

$$t \begin{cases} t_{0^o} & 0^o \leq \theta \leq 30^o \\ t_{0^o} + \dfrac{t_{60^o} - t_{0^o}}{30^o}(\theta - 30^o) & 30^o \leq \theta \leq 60^o \end{cases}$$

[b] See Figure B-26.

[c] See Figure B-27.

Implosion Results. Table B-7 summarizes the results of the analyses in terms of implosion pressures that were controlled by strain failure criteria, $(P_{im})_\varepsilon$, and stress failure criteria, $(P_{im})_\sigma$. The implosion strength is given by the nondimensional ratio of P_{im}/f'_c. The analytical implosion strength is compared to the experimental strength by the ratios shown in the last two columns of Table B-7.

The experimental specimens were out-of-round cylinders so a true comparison between analysis and experiment is only for out-of-round cylinder cases (Cases 2, 4, 6, and 8). The average ratio of strain-controlled implosion strength to experimental implosion strength was 0.89 and for stress-controlled implosion strength to experimental implosion strength was 0.93.

The stress criterion failure mode predicted implosion with better accuracy than the strain criterion method. Looking more closely at individual cases, Case 2 was an instability failure mode and analysis predicted implosion 15% lower than experimental. Cases 4, 6, and 8 were material failure modes, and analysis predicted implosion only 4% lower than experimental.

Interestingly, the strain criteria that controlled in all cases, except Case 2, was a tensile strain limit of 800 μin./in., and not a compressive strain limit. The limiting tensile strain occurred in the radial direction of the wall (increase in wall thickness) at midlength for the free-support specimens and at a distance of $\xi = 0.4$ from the end for the simple-support specimens. Tensile strain had an influence on failure because the wall thickness would laminate and facilitate a shear-compression type of material failure of the wall. Evidence of wall lamination has been observed in fragments of thick-walled spheres under hydrostatic loading (Ref 26) but was not observed in the fragments of cylinder specimens.

Table B-9. Reduction in Implosion Strength Due to Out-of-Roundness

Failure Criteria	Percent Reduction in Implosion Strength Between Case Numbers[a] –				
	1 & 2	3 & 4	5 & 6	7 & 8	Average
Strain Control	31	4	38	9	20
Stress Control	44	16	46	18	31

[a]First case number designates perfect cylinder, second case number designates out-of-round cylinder.

The effect of out-of-roundness in reducing the implosion strength of a perfectly circular cylinder is shown in Table B-9. Cylinder t/D_o influenced the out-of-roundness effect considerably. Cases 1 and 2 are thinner specimens than Cases 3 and 4, but all have a simple-support end-condition; the thinner specimens showed a 44% reduction due to out-of-roundness, whereas the thicker specimens showed a 16% reduction. A similar observation is made between Cases 5 and 6 which are thinner than Cases 7 and 8, all having a free-support end-condition.

The influence of end-condition on out-of-round effect can be observed with Cases 3 and 4 and 5 and 6, all of which have t/D_o of 0.037. Cases 3 and 4 are simply supported and showed a reduction of 16%; whereas, Cases 5 and 6 are freely supported and showed a reduction of 46%.

The effect of cylinder length can be observed from Cases 3 and 4 and 5 and 6, all of which have the same t/D_o ratio of 0.037 but different effective lengths. Cases 3 and 4 had an L/D_o ratio of 2.35, and Cases 5 and 6 had an L/D_o ratio of infinity. For the out-of-round cylinders (Cases 4 and 6), the shorter cylinder had a predicted increase in implosion strength of 53% over that of the infinitely long cylinder. Experimentally, the increase in strength was 41%.

Displacement Behavior

The predicted deflected shapes for free-support and simple-support specimens are shown in Figures B-18 and B-19. For the free-support cylinder (Figure B-18), the predicted shape is a fair approximation of the experimental shape. It should be noted that the pressure level for the experimental shape is near implosion at 400 psi (2.8 MPa) where the analytical shape is at implosion at 346 psi (2.4 MPa). For the simple-support cylinder (Figure B-19), the comparison is good.

The predicted radial displacement behavior as a function of pressure is shown in Figures B-20 and B-22. Comparison of the experimental to analytical behavior is quite good. For the out-of-round cylinders, note that the predicted implosion pressures using the strain or stress criteria are approximately the same.

A large difference in ultimate radial displacement was observed between perfect and out-of-round specimens. For cylinders of t/D_o = 0.037 (Figure B-21), the experimental out-of-round cylinder showed w = 0.508 inch (13 mm), while the perfect cylinder had w = 0.08 inch (2 mm) - a 6.4-fold increase. For specimens having the same t/D_o ratio of 0.037 but different end-support conditions (Figures B-21 and B-22), the free-support cylinders showed an ultimate displacement of w = 0.508 inch (13 mm) compared to the simple-support cylinders of w = 0.185 inch (5 mm) - a 2.7-fold increase.

Radial displacement behavior along the length of the cylinder is shown in Figures B-23 through B-25. The effect of the simple-support is vividly shown in Figures B-23 and B-25. The compliance of the actual ring stiffener in the experimental tests can be observed in Figure B-25 where approximately 0.02 inch (0.5 mm) of radial movement occurred.

For the free-support cylinder (Figure B-24), the difference between experimental and analytical behavior appears great. However, this same difference is shown in Figure B-21, where the comparison appears better. Experimentally, the free-support end-condition using a rubber gasket modeled the ideal free-support quite well.

FINDINGS

1. Analytically, using the finite element program NONSAP-A with an advanced constitutive material model, the behavior of the cylinder specimens was predicted with good accuracy. The implosion pressures were predicted 7% lower than actual when a stress criterion controlled failure. It was found experimentally that specimens of L/D_o of 2.35 had an implosion strength 41% greater than specimens of infinite length (long cylinders); analytically, the increase in strength was predicted as 53%.

2. Out-of-roundness was an important parameter in implosion strength and radial displacement behavior. Analytically, the effect of out-of-roundness was to reduce the implosion strength of perfect cylinders by 16% to 46% depending on t/D_o ratio and end-support condition. The ultimate radial displacement for the free-support experimental specimens of $t/D_o = 0.037$ was 0.508 inch (13 mm), which was 6.4 times the displacement for a perfect cylinder. The need to model out-of-roundness to obtain accurate analytical predictions was found important.

3. Radial displacement data for the specimens showed that the deflected shape for the free-support cylinders had two lobes (n = 2) and for the simple-support cylinders had three lobes (n = 3). The membrane and bending radial displacements were determined, and estimates of strain were calculated at the failure location. It appeared that at the worst flat spot the strain level at failure was slight tension on the inside wall and about 4,000 μin./in. compression on the outside wall.

LIST OF SYMBOLS

D_o	Outside diameter
E_i	Initial elastic modulus
E_s	Secant elastic modulus
E_t	Tangent elastic modulus
f'_c	Uniaxial concrete compressive strength
k_c	Material strength factor for cylinder structures
k_s	Material strength factor for spherical structures
L	Cylinder length
n	Number of lobes
P	External pressure
P_{im}	Implosion pressure
$(P_{im})_\varepsilon$	Analytical implosion pressure controlled by strain criteria
$(P_{im})_\sigma$	Analytical implosion pressure controlled by stress criteria
R	Average radius
R_o	Outside radius
t	Average wall thickness
t_{min}	Minimum wall thickness
w	Radial displacement from initial to deflected shape
w_b	Bending radial displacements
w_m	Membrane radial displacements
w_T	Total radial displacement (see Figure B-17)
ΔR	Deviation in radius
ΔR_i	Inside deviation from average radius
ΔR_o	Outside deviation from average radius
Δt_{min}	$t - t_{min}$
ε_u	Ultimate strain
ε_b	Bending strain
ε_m	Membrane strain
η	Empirical plasticity reduction factor
θ	Angular coordinate (see Figures B-26 and B-27)
θ_1, θ_2	Angular coordinates of failure zone
θ_3	Angular coordinate of center of failure zone
ν	Poisson's ratio
ξ	Nondimensional distance along cylinder length (see Figure B-4)
σ	Wall stress
σ_{im}	Wall stress at implosion
$(\sigma_{im})_B$	Wall stress at implosion predicted by Bresse's equation (Equation 5)
$(\sigma_{im})_D$	Wall stress at implosion predicted by Donnell's equation (Equation 4)
ϕ	Ratio of radial displacements between end and middle of cylinder

DISTRIBUTION LIST

ARMY CRREL Library, Hanover NH
ARMY ENG WATERWAYS EXP STA Library, Vicksburg MS
BUREAU OF RECLAMATION (J Graham), Denver, CO; G. Smoak, Denver CO
CNO Code OPNAV 22, Wash DC; Code OPNAV 23, Wash DC; OP-23 (Capt J.H. Howland) Washinton, DC
COMOCEANSYSPAC SCE, Pearl Harbor HI
COMSUBDEVGRUONE Operations Offr, San Diego, CA
DNA (LTCOL J. Galloway), Washington, DC
DNL Washington DC
DOE (D Uthus), Arlington, VA; (G. Boyer), Washington, DC; (W. Sherwood) Washington, DC; Dr. Cohen
DTNSRDC Code 172 (M. Krenzke), Bethesda MD
DTNSRDC Code 522 (Library), Annapolis MD
ENVIRONMENTAL PROTECTION AGENCY (Dr. R Dyer), Washington, DC
MARINE CORPS BASE PWO Camp Lejeune NC
MARITIME ADMIN (E. Uttridge), Washington, DC
MCAS CO, Kaneohe Bay HI
MCRD PWO, San Diego Ca
NAVCOASTSYSTCTR Code 713 (J. Quirk) Panama City, FL; Library Panama City, FL
NAVEODFAC Code 605, Indian Head MD
NAVFACENGCOM Code 042 Alexandria, VA; Code 0453 (D. Potter) Alexandria, VA; Code 0454B Alexandria, Va; Code 04B (M. Yachnis) Alexandria, VA; Code 04B5 Alexandria, VA
NAVFACENGCOM - CHES DIV. Code FPO-1 Wash, DC
NAVOCEANO Code 1600 Bay St. Louis, MS
NAVOCEANSYSCEN Code 5204 (J. Stachiw), San Diego, CA; Code 93, San Diego, CA
NAVPGSCOL (Dr. G. Haderlie), Monterey, CA; J. Garrison Monterey CA
NAVPHIBASE Harbor Clearance Unit Two, Little Creek, VA
NAVREGMEDCEN SCE, Guam; SCE, Philadelphia PA
NAVSEASYSCOM (R. Sea), Washington, DC; Code 0353 (J. Freund) Washington, DC; Code SEA OOC Washington, DC
NAVSEC Code 6034, Washington DC
NAVSURFWPNCEN J. Honaker, White Oak Lab, Silver Spring, MD
NAVTECHTRACEN SCE, Pensacola FL
NAVWARCOL President, Newport, RI
NAVWPNCEN ROICC (Code 702), China Lake CA
NCBC Code 155, Port Hueneme CA
NOAA (Dr. T. Mc Guinness) Rockville, MD; (M. Ringenbach), Rockville, MD
NRL Code 8400 Washington, DC
NUCLEAR REGULATORY COMMISSION T.C. Johnson, Washington, DC
NUSC Code S332, B-80 (J. Wilcox)
OCEANAV Mangmt Info Div., Arlington VA
ONR (Dr. E.A. Silva) Arlington, VA
SUBRESUNIT OIC Seacliff, San Diego; OIC Turtle, San Diego
PETRO MARINE ENGINEERS EDI
U.S. MERCHANT MARINE ACADEMY Kings Point, NY (Reprint Custodian)
US GEOLOGICAL SURVEY (F Dyhrkopp) Metairie, LA; (R Krahl) Marine Oil & Gas Ops, Reston, VA
USAF SCHOOL OF AEROSPACE MEDICINE Hyperbaric Medicine Div, Brooks AFB, TX
USNA Ocean Sys. Eng Dept (Dr. Monney) Annapolis, MD; Oceanography Dept (Hoffman) Annapolis MD
BROOKHAVEN NATL LAB M. Steinberg, Upton NY
CALIFORNIA STATE UNIVERSITY LONG BEACH, CA (YEN); LOS ANGELES, CA (KIM); Long Beach, CA (Kendall)
CLARKSON COLL OF TECH G. Batson, Potsdam NY
DAMES & MOORE LIBRARY LOS ANGELES, CA
DUKE UNIV MEDICAL CENTER B. Muga, Durham NC
UNIVERSITY OF DELAWARE (Dr. S. Dexter) Lewes, DE
FLORIDA ATLANTIC UNIVERSITY Boca Raton FL (Ocean Engr Dept., C. Lin)
FLORIDA ATLANTIC UNIVERSITY Boca Raton FL (W. Tessin)
FLORIDA ATLANTIC UNIVERSITY W. Hartt, Boca Raton FL

FLORIDA INSTITUTE OF TECHNOLOGY (J Schwalbe) Melbourne, FL
GEORGIA INSTITUTE OF TECHNOLOGY Atlanta GA (School of Civil Engr., Kahn)
HOUSTON UNIVERSITY OF (Dr. R.H. Brown) Houston, TX
INSTITUTE OF MARINE SCIENCES Dir. Port Aransas TX
JOHNS HOPKINS UNIV Rsch Lib, Baltimore MD
LEHIGH UNIVERSITY BETHLEHEM, PA (MARINE GEOTECHNICAL LAB., RICHARDS); Bethlehem PA (Fritz Engr. Lab No. 13, Beedle)
LIBRARY OF CONGRESS WASHINGTON, DC (SCIENCES & TECH DIV)
MAINE MARITIME ACADEMY (Wyman) Castine ME
MIT Cambridge MA
NATL ACADEMY OF ENG. ALEXANDRIA, VA (SEARLE, JR.)
NORTHWESTERN UNIV Z.P. Bazant Evanston IL
UNIV. NOTRE DAME Katona, Notre Dame, IN
OKLAHOMA STATE UNIV (J.P. Lloyd) Stillwater, OK
PURDUE UNIVERSITY W. Chen, West Lafayette, IN
MUSEUM OF NATL HISTORY San Diego, CA (Dr. E. Schulenberger)
SCRIPPS INSTITUTE OF OCEANOGRAPHY San Diego, CA (Marina Phy. Lab. Spiess)
SEATTLE U Prof Schwaegler Seattle WA
SOUTHWEST RSCH INST R. DeHart, San Antonio TX
STANFORD UNIVERSITY Stanford CA (Gene)
STATE UNIVERSITY OF NEW YORK (Dr. H. Herman) Stony Brook, NY
TEXAS A&M UNIVERSITY College Station, TX Depts of Ocean. & Meteor; W.B. Ledbetter College Station, TX
UNIV. AKRON T.Y. Change, Akron, OH
UNIVERSITY OF CALIFORNIA Berkeley CA (B. Bresler); Berkeley CA (D.Pirtz); Berkeley CA (Dept of Naval Arch.); Engr Lib., Berkeley CA; M. Duncan, Berkeley CA; P. Mehta, Berkeley CA
UNIVERSITY OF DELAWARE Newark, DE (Dept of Civil Engineering, Chesson)
UNIVERSITY OF HAWAII Honolulu HI (Dr. Szilard)
UNIVERSITY OF ILLINOIS Metz Ref Rm, Urbana IL; URBANA, IL (NEWMARK); Urbana IL (CE Dept, W. Gamble)
UNIVERSITY OF MASSACHUSETTS (Heronemus), Amherst MA CE Dept
UNIVERSITY OF MICHIGAN Ann Arbor MI (G. Berg); Ann Arbor MI (Richart)
UNIVERSITY OF NEW HAMPSHIRE DURHAM, NH (LAVOIE)
UNIVERSITY OF TEXAS AT AUSTIN Austin, TX (Breen)
UNIVERSITY OF TEXAS MEDICAL BRANCH (Dr. R.L. Yuan) Arlington, TX
UNIVERSITY OF WASHINGTON (Dr. N. Hawkins) Seattle, WA; Dept of Civil Engr (Dr. Mattock), Seattle WA; Seattle WA (E. Linger)
WOODS HOLE OCEANOGRAPHIC INST. Doc Lib LO-206, Woods Hole MA
AGBABIAN ASSOC. C. Bagge, El Segundo CA
ALFRED A. YEE & ASSOC. Honolulu HI
AMERICAN BUR OF SHIPPING (S Stiansen) New York, NY
APPLIED TECH COUNCIL R. Scholl, Palo Alto CA
ARVID GRANT OLYMPIA, WA
AUSTRALIA A. Eddie, Victoria
BECHTEL CORP. R. Leonard, San Francisco CA
BELGIUM Gent (N. De Meyer); HAECON, N.V., Gent
BRAND INDUS SERV INC. J. Buehler, Hacienda Heights CA
CANADA Library, Calgary, Alberta; Lockheed Petro. Serv. Ltd, New Westminster B.C.; M. Malhotra, Ohawa, Canada; Surveyor, Nenninger & Chenevert Inc., Montreal; W. German, Montreal, Quebec
CF BRAUN CO Du Bouchet, Murray Hill, NJ
CHAS. TL MAIN, INC. (R.C. Goyette), Portland, OR
COLUMBIA GULF TRANSMISSION CO. HOUSTON, TX (ENG. LIB.)
CONCRETE TECHNOLOGY CORP. TACOMA, WA (ANDERSON)
CONRAD ASSOC. Van Nuys CA (W. Gates)
CONTINENTAL OIL CO O. Maxson, Ponca City, OK
DENMARK E. Wulff, Svenborg
DILLINGHAM PRECAST F. McHale, Honolulu HI
DIXIE DIVING CENTER Decatur, GA
EXXON Production Research Co. Runge, Houston, TX
EXXON PRODUCTION RESEARCH CO Houston, TX (Chao)

FRANCE (J. Trinh) ST-REMY-LES-CHEVREUSE; (P Ozanne), Brest; Dr. Dutertre, Boulogne; L. Pliskin, Paris; P. Jensen, Boulogne; P. Xercavins, Europe Etudes; Roger LaCroix, Paris
GERMANY C. Finsterwalder, Sapporobogen 6-8
GLOBAL ASSOCIATES Engr Dept (Scott), Kwajalein
GULF RAD. TECH. San Diego CA (B. Williams)
INDIA Shri J. Bodhe, Fort Bombay
ITALY M. Caironi, Milan; Torino (F. Levi)
JAPAN (Dr. T. Asama), Tokyo; M. Kokubu, Tokyo; S. Inomata, Tokyo; S. Shiraishi, Tokyo
LIN OFFSHORE ENGRG P. Chow, San Francisco CA
LOCKHEED MISSILES & SPACE CO. INC. L. Trimble, Sunnyvale CA
MC CLELLAND ENGINEERS INC Houston TX (B. McClelland)
MEXICO R. Cardenas
MOBIL R & D CORP (J Hubbard), Dallas, TX
NEW ZEALAND New Zealand Concrete Research Assoc. (Librarian), Porirua
NOBLE, DENTON & ASSOC., INC. (Dr. M Sharples) Houston, TX
NORWAY E. Gjorv, Trondheim; F. Manning, Stavanger; J. Creed, Ski; Norwegian Tech Univ (Brandtzaeg), Trondheim; P.S. Hafskjold, Oslo; R. Sletten, Oslo; S. Fjeld, Oslo; Siv Ing Knut Hove, Oslo
OFFSHORE POWER SYS (S N Pagay) Jacksonville, FL
PACIFIC MARINE TECHNOLOGY Long Beach, CA (Wagner)
PORTLAND CEMENT ASSOC. (Dr. E. Hognestad) Skokie, IL; SKOKIE, IL (CORLEY; Skokie IL (Rsch & Dev Lab, Lib.)
PRESTRESSED CONCRETE INST C. Freyermuth, Chicago IL
SANDIA LABORATORIES (Dr. D.R. Anderson) Albuquerque, NM
SCHUPACK ASSOC SO. NORWALK, CT (SCHUPACK)
SHELL OIL CO. HOUSTON, TX (WARRINGTON); I. Boaz, Houston TX
SOUTH AMERICA B. Contarini, Rio de Janeiro, Brazil; N. Nouel, Valencia, Venezuela
SPAIN D. Alfredo Paez, Algorta
SWEDEN Cement & Concrete Research Inst., Stockholm; GeoTech Inst; K. Christenson, Stockholm; Kurt Eriksson, Stockholm
THE NETHERLANDS Ir Van Loenen, Beverwijk; J. Slagter, Driebergen
TRW SYSTEMS REDONDO BEACH, CA (DAI)
UNITED KINGDOM (D. Faulkner) Glasgow, Scotland; (Dr. F.K. Garas), Middlesex; (Dr. P. Montague) Manchester, England; (H.W. Baker) Glasgow, Scotland; (M E W Jones) Glasgow, Scotland; (M J Collard), London; A. Denton, London; Cambridge U (Dr. C. Morley) Cabridge, GB; Cement & Concrete Assoc Wexham Springs, Slough Bucks; Cement & Concrete Assoc. (Lit. Ex), Bucks; Cement Marketing Co. Ltd. (Brittain) London; D. Lee, London; J. Derrington, London; Library, Bristol; P. Shaw, London; R. Browne, Southall, Middlesex; Sunderland Polytechnic (A.L. Marshall), Great Britain; T. Ridley, London; Taylor, Woodrow Constr (Stubbs), Southall, Middlesex; Univ. of Bristol (R. Morgan), Bristol; W. Crozier, Wexham Springs; Watford (Bldg Rsch Sta, F. Grimer)
WOODWARD-CLYDE CONSULTANTS PLYMOUTH MEETING PA (CROSS, III)
BROWN, ROBERT University, AL
DOBROWOLSKI, J.A. Altadena, CA
GERWICK, BEN C. JR San Francisco, CA
LAYTON Redmond, WA
NORWAY B. Nordby, Oslo
WATT BRIAN ASSOC INC. Houston, TX
WESTCOTT WM Miami, FL
WM TALBOT Orange CA

DEPARTMENT OF THE NAVY

CIVIL ENGINEERING LABORATORY
NAVAL CONSTRUCTION BATTALION CENTER
PORT HUENEME, CALIFORNIA 93043

OFFICIAL BUSINESS
PENALTY FOR PRIVATE USE, $300

POSTAGE AND FEES PAID
DEPARTMENT OF THE NAVY
DoD-316